A Time–Frequency Analysis on the Impact of Climate Variability on Semi-Natural Mountain Meadows

Mario Cunha and Christian Richter

***Abstract*—This paper analyzes the impact of climate dynamics on vegetation growth for a rural mountainous region in northeastern Portugal. As a measure of vegetation growth, we use the normalized difference vegetation index (NDVI), which is based on the ten-day synthesis data set (S10) from Satellite Pour l'Observation de la Terre (SPOT-VEGETATION) imagery from 1998 to 2011. We test whether the dynamic growth pattern of the NDVI has changed due to climate variability, and we test the relationship of NDVI with temperature and available soil water (ASW). In order to do so, we use a time–frequency approach based on Kalman filter regressions in the time domain. The advantage of our approach is that it can be used even in the case where the sample size is relatively small. By estimating the important relationships in the time domain first and transferring them into the frequency domain, we are still able to derive a complete spectrum over all frequencies. In our example, we find a change of the cyclical pattern for the spring season and different changes if we take into account all seasons. In other words, we can distinguish between deterministic changes of the vegetation cycles and stochastic changes that only occur randomly. Deterministic changes imply that the data-generating process has changed (such as climate), whereas stochastic changes imply only temporary changes. We find that individual seasons undergo cyclical changes that are different from other seasons. Moreover, our analysis shows that temperature and ASW are the main drivers of vegetation growth. We can also recognize a shift of the relative importance away from temperature to soil water.**

***Index Terms*—Climate variability, Kalman filter, mountain meadows, normalized difference vegetation index (NDVI), time-varying spectra, vegetation dynamics.**

I. Introduction

TIME–frequency analysis is used in engineering for quite some time [1]. Time–frequency analysis investigates cycles whose properties may change over time. The inspiration for this paper is therefore to investigate whether climate change has a (changing) impact on natural growth cycles. Climate changes are particularly serious for mountainous regions because they are among the most fragile environments in the world [2], [3] and are recognized as the key supporting ecosystem service related to natural resources conservation, as defined by the Millennium Ecosystem Assessment [4]. Therefore, if climate change has an impact on growth cycles, it should be measurable in a sensitive system such as mountainous regions. As an example, we study the mountainous grassland system in northeast Portugal. The traditional landscape of the mountainous region of northeastern Portugal is characterized by the ancestral agropastoral or grassland system extensively used for hay and grazing. The increased water constrains due to sectorial competition for water uses and the foreseeable climate warming endangers the sustainability of these lameiros. Hence, our results may be also used for conservation strategies to preserve these meadows.

Remote sensing of vegetation dynamics at regional and field scales is often pursued using high-temporal-resolution sensors [advanced very high resolution radiometer, medium resolution imaging spectrometer, moderate resolution imaging spectroradiometer, and Satellite Pour l'Observation de la Terre (SPOT-VEGETATION)]. The data received from these sensors provide large area coverage with high frequency, limited only by the compositing period needed to remove the effects of clouds and cloud shadow [5]–[7]. Results from previous works show that the normalized difference vegetation index (NDVI) profile provided by the VEGETATION sensor, on board the most recent SPOT—SPOT_VGT—fits well the characteristics of vegetation growth dynamics and associated management practices in the semi-natural meadows of the mountainous region of northeast Portugal [8]–[10]. Hence, in this paper, we use the NDVI time series based on SPOT_VGT sensor imagery to infer about the impact of climate on these semi-natural meadows and to model vegetation dynamics.

Several approaches based on temporal trajectory analysis have been proposed for smoothing and detecting temporal changes in vegetation dynamics such as change vector analysis [11], Best Index Slope Extraction [12], moving averages [13], double logistic model [14], asymmetric Gaussian [15], sliding windows [16], wavelet decomposition [17], harmonic series and higher order splines [18], [19], Breaks For additive Seasonal and Trend [20], Whittaker smoother [21], changing-weight filter [22], discrete Fourier transform [23], and frequency analysis [24]. Many of these techniques need complementary complicate and tedious tests (e.g., derivatives, specific threshold, or change trajectories) to extract the time-series changes. Reviews of the merits and limitations of these techniques can be found in [18], [21], [22], and [24]–[26]. According to this literature, stationarity assumptions, data quality, sensor noise, and complications of the methods can make it challenging to quantify the separate sources of information that influence the signal and

Manuscript received January 9, 2013; revised June 19, 2013 and November 2, 2013; accepted November 23, 2013.

M. Cunha is with the Centro de Investigação em Ciências Geo-Espaciais, Faculdade de Ciências, Universidade do Porto, 4485-661 Vairão, Portugal (e-mail: mcunha@mail.icav.up.pt).

C. Richter is with the University of Bedfordshire Business School, University of Bedfordshire, Bedfordshire LU1 3JU, U.K. (e-mail: Christian.Richter@beds.ac.uk).

Color versions of one or more of the figures in this paper are available online at http://ieeexplore.ieee.org.

Digital Object Identifier 10.1109/TGRS.2013.2295321

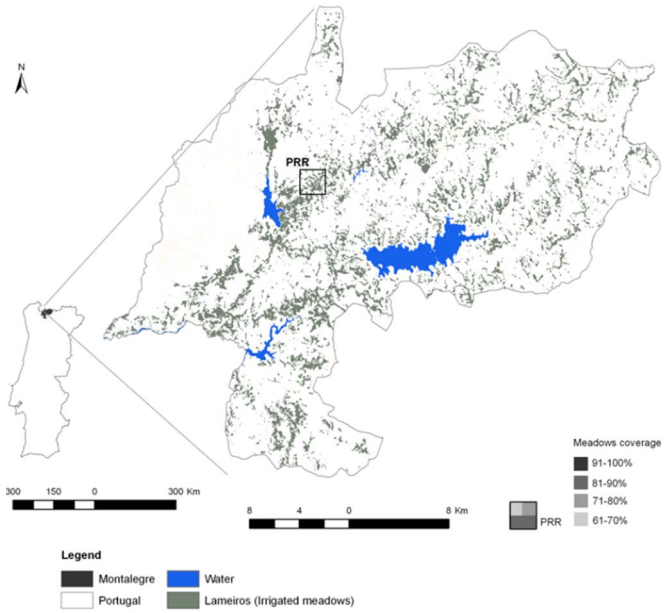

Fig. 1. Location of the study area (Montalegre) in northeast Portugal and the test site located in PRR, showing the meadow coverage in Montalegre (in gray). The PRR (2 × 2 pixels) coordinates (Datum WGS84) of the upper left site corner are 7°55′04 W and 41°48′32″ N. Details of meadow coverage per pixel in the test site are also given as percentages.

to determine what constitutes a significant change. Moreover, the frequently used time-series analysis of satellite derived vegetation growth data (e.g., [8], [27]) are not capable to integrate and quantify the seasonal and interannual impacts of climate on vegetation dynamics.

It is well known that vegetation dynamics depend on the climate. However, an open question is how sensitive are seasonal and interannual cycles to climate variability. Therefore, a time-varying spectral approach, which is capable of separating out changes at different cyclical frequencies (including trend) in the grassland growth, is needed to provide the flexibility to capture these features.

We identify the importance of variability of climate for cyclical properties in the satellite-based grassland growth rate and consider how the impacts of these events may be predicted. The following section describes the test site and the methods used to derive the data. Section III briefly explains the statistical methods used in this paper. Section IV gives the results. A discussion is provided in Section V, and Section VI concludes this paper.

II. Materials and Methods

A. Study Area

The region of analysis covers a large area of the mountainous region of Montalegre, northeast Portugal (see Fig. 1).

The large pixel size of SPOT_VGT images (1 km) determines the criteria for selection of the test site, which have to include large contiguous areas with lameiros fields. Therefore, one suitable test site was selected in Montalegre municipality, location of Paredes do Rio (PRR). The test sites have 2 × 2 pixels (of 1 × 1 km), in a compact group of contiguous pixels, all with 65% or more lameiros coverage. The average lameiros coverage occupancy of the PRR test site is 77.8% (see Fig. 1).

These meadows are conveniently located in areas of high water availability, loamy soils, and over 700–800 m high. In this region, the Atlantic climate favors high precipitation occurrence (1531 mm/year), mainly occurring from autumn to spring, autumn–winter temperatures lower than 12 °C. and mean monthly temperatures ranging from 3.5 °C to 17.2 °C.

B. Meteorological Data and Soil Water Balance

We use meteorological observations for the years 1998 to 2011 from the weather station of Montalegre (41°49′ N : 7°47′ W: 1005 m above sea level) located in the proximity of the test site. The meteorological data consist of daily observations of temperature (maximum and minimum) and precipitation. These general meteorological parameters are used to derive other variables: mean temperature (Tm, °C), potential evapotranspiration (ETP, mm), and other variables related to soil water balance.

The Thornthwaite–Matter (T–M) [28] mass conservation climatic water budget model is then performed to simulate ten-day soil water balance. Dekadal ETP is estimated using the empirical Thornthwaite equation that relies on mean temperature and average day length (in hours per day). The T–M model tracks the soil water through time by balancing the inputs (precipitation) and outputs of water (ETP). The soil operates as a "bucket" with a user-defined field available water capacity: 100 mm in this study. The ability to remove soil moisture has been set to decrease exponentially with the decreasing soil-moisture content. The model output includes available soil water (ASW) that ranges from 0 to 100 mm. This methodology was chosen because of its simplicity and small quantity of input meteorological data needed.

C. Satellite Data

In this paper, we use the satellite imagery provided by SPOT_VGT for the period 1998 (April) to 2011 (March) to examine the dynamic patterns of grassland grow inferred by the NDVI. This satellite has an intermediate spatial resolution (1 km), and the images are corrected for radiometric, geometric, and atmospheric effects. Ten-day composite VEGETATION products (S10) are obtained from the compilation of daily data. In the SPOT_VGT S10 composites, the resulting surface reflectance value for each pixel corresponds to the date with the maximum NDVI reflectance at the top of the atmosphere for that pixel [29].

The pixels of the test site (2 × 2 pixels) were averaged to create the NDVI value for each time period. This was done to prevent misregistration and errors from other sources; these errors could contaminate the temporal profiles.

The NDVI is a variable that is truncated (it can only adopt values between −1 and 1). In a truncated sample, information on the regressors is available only if the regressand is actually observed. In our example, we cannot observe values of the NDVI below −1 and above 1 (may be seen as a truncated distribution), which results in a nonnomal distribution [30]. This implies that either one has to adopt an estimation technique that takes truncated variables into account or we have to transform NDVI data into a nontruncated variable. For this reason, we transformed NDVI into a growth rate. This growth rate is not truncated anymore; thus, common estimation techniques can be used. Given our data set, we can construct different growth

rates. We have tested these different growth rates such as ten-day growth rates and monthly growth rates, but we found that the model using the annual growth rate was statistically superior to all other models in the sense that it minimized the Akaike and Schwartz information criteria [31]. We calculated the annual growth rate in the following way: we first calculated for all observations of NDVI the annual growth rate. In accordance with the seasonal calendar, we then calculated the average annual growth rate for a particular season. Therefore, in this paper, we work with average data on seasonal level, and we use annual growth rates rather than level values.

To make the approach consistent, we also use the same growth rates for temperature and soil water. Hence, in all regressions to come, all variables refer to the same time period and have the same dimension, namely, percent.

III. Time–Frequency Analysis of the NDVI

A. First Step: Estimation in the Time Domain

In contrast to "common" frequency approaches, we do not estimate the spectrum directly. The reason is that this usually requires a large number of observations. If one takes into account nonstationary spectra as well, then the number of necessary observations increases even more. By estimating a time-series model, first, we avoid this problem. Moreover, an important advantage of our approach is that we can *calculate* a spectrum showing *all* frequencies (even the long ones) with a relatively small sample size. We can further test whether the properties of the long cycles may have changed over the sample period. Thus, our conclusions concerning the long-run (and short-run) cycle properties are only valid for the sample under consideration and may change afterward or have been different before our sample. The crucial point is, however, that we can infer from small-sample long-run cycle properties.

In the first step, we estimate the cyclic behavior of the growth rate of each individual variable, i.e., NDVI, ASW, and Tm. In order to do so, we have to estimate an autoregressive model of order p, i.e., AR(p), where p is determined by statistical tests. In order to allow for the possible changes in the parameters, we will employ a time-varying model AR(p) by applying a Kalman filter to the chosen model as follows:

$$y_t = \alpha_{0,t} + \sum_{i=1}^{9} \alpha_{i,t} y_{t-i} + \varepsilon_t \tag{1}$$

where y_t is the NDVI growth rate, and

$$\alpha_{i,t} = \alpha_{i,t-1} + \eta_{i,t}, \qquad \text{for } i = 0, \ldots, 9 \tag{2}$$

and $\varepsilon_t, \eta_{i,t} \sim$ i.i.d.$(0, \sigma^2_{\varepsilon,\eta_i})$, for $i = 0, \ldots, 9$.

α_s are the unknown coefficients to be estimated. We employ a general to specific approach (starting with $p = 9$) to obtain a final specification for (1), eliminating insignificant lags. The maximum number of lags was determined by the Akaike information criterion (AIC). For each regression, we applied a set of diagnostic tests, as shown in Tables I–III, to confirm the final specification found.

Using the aforementioned specification implies that we get a set of parameter values for each point in time (here, a point in time is one season). Hence, a particular parameter could be significant for all points in time or at some periods but not others, or it might never be significant. These parameter changes are at the heart of this paper as they imply changes in the lag structure and, hence, changes in the spectral results. If

TABLE I
Regression Results for *dl*NDVI

Estimation by Kalman Filter			
Dependent Variable	dlNDVI		
Usable Observations	48	Degrees of Freedom	45
R2	0.99308		
Mean of Dep.Variable	0.00356	Std Error of dep. variable	0.054619
Standard Error of Estimate	0.051779	SS Residuals	0.093837
Akaike Information Criterion	0.06117	Ljung-Box Test: Q*(9) =	13.3008
Variable	Coeff	Std Error	T-Stat
Constant	-0.0113	0.0441	-0.2559
dlNDVI {3}	0.1260	0.0330	3.8128
dlNDVI {4}	-0.4198	0.0641	-6.5492
dlNDVI {8}	-0.2358	0.0706	-3.3410

Annual growth rate of NDVI (dlNDVI)

TABLE II
Regression Results Between *dl*NDVI and Temperature

Estimation by Kalman Filter			
Dependent Variable	dlNDVI		
Usable Observations	48	Degrees of Freedom	42
R2	0.97282		
Mean of Dependent Variable	0.0036	Std Error of dep. variable	0.0546
Standard Error of Estimate	0.0779	Sum of Squared Residuals	0.1943
Akaike Information Criterion	0.1043	Ljung-Box Test: Q*(9) =	16.4616.
Variable	Coeff	Std Error	T-Stat
Constant	-0.0116	0.0352	-0.3305
dlNDVI {4}	-0.7842	0.0925	-8.4767
dlNDVI {8}	-0.1021	0.0400	-2.5526
dlTmed	0.0863	0.0182	4.7353
dlTmed {3}	0.0978	0.0210	4.6718
dtTmed {4}	-0.1112	0.0305	-3.6415
dlTmed {7}	-0.0823	0.0228	-3.6076

Annual growth rate of NDVI (dlNDVI)

TABLE III
Regression Results Between *dl*NDVI and ASW

Estimation by Kalman Filter			
Dependent Variable	dlNDVI		
Usable Observations	48	Degrees of Freedom	42
R2	0.97282		
Mean of Dependent Variable	0.0036	Std Error of dep. variable	0.0546
Standard Error of Estimate	0.0779	Sum of Squared Residuals	0.1943
Akaike Information Criterion	0.1043	Ljung-Box Test: Q*(9) =	16.4616.
Variable	Coeff	Std Error	T-Stat
Constant	-0.0116	0.0352	-0.3305
dlNDVI {4}	-0.7842	0.0925	-8.4767
dlNDVI {8}	-0.1021	0.0400	-2.5526
dlTmed	0.0863	0.0182	4.7353
dlTmed {3}	0.0978	0.0210	4.6718
dtTmed {4}	-0.1112	0.0305	-3.6415
dlTmed {7}	-0.0823	0.0228	-3.6076

Annual growth rate of NDVI (dlNDVI)

a parameter was significant for some periods but not others, it was kept in the equation with a parameter value of zero for those periods in which it was insignificant. This strategy minimized the AIC and led to a parsimonious specification. Finally, we tested the residuals in each regression for autocorrelation and heteroscedasticity.

The final specification [see (1) and (2)] was then *validated* using two different stability tests. The first is the fluctuation test in Ploberger *et al.* [32], which detects *discrete* breaks at any point in time in the coefficients of a (possibly dynamic) regression. The second test is due to LaMotte and McWorther [33] and is specifically designed to detect *random* parameter variation of a specific unit root form (our specification). We found that the random walk hypothesis for the parameters was justified for each model (results available on request). We also test for autocorrelation of the residuals. For this purpose, we use the Ljung–Box test, which allows for autocorrelated residuals of order p. In all our regressions, we could reject the hypothesis of autocorrelation.

It should be noted that all our tests of significance and significant differences in parameters are being conducted in the time domain *before* transferring to the frequency domain. This is because no statistical tests exist for calculated spectra (the data transformations are nonlinear and involve complex arithmetic). Stability tests are important here because our spectra are sensitive to changes in the underlying parameters. However, given the extensive stability and specification tests conducted, we know there is no reason to switch to another model that fails to pass those tests.

Once this regression is done, it gives us a time-varying AR(p) model. From this AR(p) we can then *calculate* the short–time Fourier transform as outlined below, and as originally suggested by Gabor [34], in order to *calculate* the associated time-varying spectrum.

B. Second Step: Spectrum Analysis

Having estimated the time-series model, we are now able to analyze the power spectral density (PSD) function of the growth rate of NDVI. The PSD function shows the strength of the variations (energy) of a time series at each frequency of oscillation. In the diagram, it shows at which frequency variations are strong/powerful and at which frequencies the variations are weak (expressed in "energy"). The unit of measurement in the PSD is energy (variance) per frequency, frequency band, or cycle length.

In order to calculate the spectrum from an estimated representation of (1), we use the fast Fourier transform (FFT). Using the FFT, the time-varying spectrum of the growth rate series can be calculated as follows [35]:

$$P_t(\omega) = \frac{\sigma^2}{\left|1 + \sum_{i=1}^{9} \alpha_{i,t} \exp(-j\omega i)\right|_t^2} \tag{3}$$

where ω is the angular frequency, and j is a complex number. The main advantage of this method is that, at any point in time, a power spectrum can be instantaneously calculated from the updated parameters of the model. Hence, we are able to generate a power spectrum even if we have a short time series and even if that time series contains structural breaks.

C. Third Step: Cross-Spectrum Analysis

In this paper, we also investigate the linkage between different NDVI-based vegetation growth cycles. In the frequency domain, the natural tool to do that is the coherence.

Suppose now we are interested in the relationship between two variables $\{y_t\}$ and $\{x_t\}$, where $\{y_t\}$ is the grass growth rate and $\{x_t\}$ is the temperature variability, for example. We can then estimate an autoregressive distributed lag model (ARDL(p, q) of the order (p, q), where p gives the number of lags of the endogenous variable and q gives the number of lags of the exogenous variable. Using the lag polynomial, we can write the (ARDL(p, q) model in general terms as follows:

$$V(L)_t y_t = A(L)_t x_t + u_t, u_t \sim \text{i.i.d.}(0, \sigma^2) \tag{4}$$

where $A(L)_t$ and $V(L)_t$ are filters, and L is the lag operator such that $\text{L}z_t = z_{t-1}$. Notice that the lag structures $A(L)_t$ and $V(L)_t$ are time varying. That means we need to use a state-space model (we use the Kalman filter again) to estimate the implied lag structure. That is

$$\begin{aligned} v_{i,t} &= v_{i,t-1} + \varepsilon_{i,t}, \text{ for } i = 1, \ldots, p \text{ and } \varepsilon_{i,t} \sim \left(0, \sigma^2_{\varepsilon_i}\right) \\ a_{i,t} &= a_{i,t-1} + \eta_{i,t}, \text{ for } i = 0, \ldots, q \text{ and } \eta_{i,t} \sim \left(0, \sigma^2_{\eta_i}\right). \end{aligned} \tag{5}$$

As before, we test for the random walk property using the LaMotte–McWorther test. In addition, for structural breaks, we employ the fluctuation test [32]. Finally, we use our previous general-to-specific approach to estimate (4), starting off with lag lengths of 9 and $p = q$, and dropping those lags that were never significant (as we did before).

Having estimated the coefficients in (4), we can calculate the gain, coherence, and cross spectra based on the time-varying spectra just obtained. A direct estimation of the cross spectra is a particular problem in the case of structural breaks since the subsamples would typically be too small to allow the associated spectra to be directly estimated.

For the cross-spectral analysis, we use the methods introduced in Hughes Hallett and Richter [36]–[38]. The time-varying cross spectrum $f_{YX}(\omega)_t$ using the FFT can be written as

$$f_{YX}(\omega)_t = |T(\omega)|_t \, f_{XX}(\omega)_t \tag{6}$$

where $T(\omega)_t$ is the transfer or filter function defined in (6) and calculated as follows:

$$T(\omega)_t = \left(\frac{\sum_{b=0}^{q} a_{b,t} \exp(-j\omega b)}{1 - \sum_{i=1}^{p} v_{i,t} \exp(-j\omega i)} \right), \text{ for } t = 1, \ldots, T. \tag{7}$$

In (7), a's and v's are estimated using (4). The last term in (6), i.e., $f_{XX}(\omega)_t$, is the spectrum of the predetermined variable. This spectrum may be time varying as well (see above). However, in this paper, we are interested in the coherence and in the composition of the changes to that coherence over time. Thus, we need to establish expressions for the coherence and gain between x_t and y_t to show the degree of association and size

of impact of x_t on y_t. The spectrum of any dependent variable is defined as (e.g., [39])

$$f_{YY}(\omega)_t = |T(\omega)_t|^2 \; f_{XX}(\omega)_t + f_{vv}(\omega)_t. \tag{8}$$

From (3), we get the time-varying residual spectrum

$$f_{vv}(\omega)_t = \frac{f_{uu}(\omega)_t}{\left|1 - \sum_{i=1}^{p} v_{i,t} \exp(-j\omega i)\right|^2} \tag{9}$$

and the gain as $A(\omega)_t = |T(\omega)_t|^2$ and is calculated as described in (7).

Finally, given knowledge of $f_{YY}(\omega)_t$, $|T(\omega)_t|^2$, and $f_{XX}(\omega)_t$, we can *calculate* the coherence at each frequency as follows (as defined in Hughes Hallett and Richter [37], [40]:

$$K^2_{YX,t} = \frac{1}{\left\{1 + f_{VV}(\omega)_t / \left(|T(\omega)_t|^2 f_{XX}(\omega)_t\right)\right\}}. \tag{10}$$

The spectral coherence K^2_{XY} is a statistic that can be used to examine the relation between two signals or data sets. Values of the coherence will always satisfy $0 \leq K^2_{XY} \leq 1$. For a strictly proportional linear system with a single input x_t and single output y_t, the coherence will be equal to one. If x_t and y_t are completely unrelated, then the coherence will be zero. If K^2_{XY} is less than one but greater than zero, it is an indication that output y_t is being produced by input x_t, as well as by other inputs. Hence, the coherence is nothing else than the R^2 in the frequency domain. Since we are calculating the coherence using the short-time Fourier transform, the coherence may be also time varying. Thus, we have to extend K^2_{XY} by a time index. For the rest of this paper, we will write $K^2_{XY,t}$.

For example, if the coherence has a value of 0.6 at a frequency of 1.2, then it means that the temperature cycle at a frequency of 1.2 determines an NDVI-based vegetation growth cycle at that point in time by 60%. Similarly, a gain of 0.5 means that half the variance in temperature cycle at that frequency is transmitted to the NDVI.

IV. Results

A. NDVI-Based Growth of Semi-Natural Grassland and Climate

As mentioned before, instead of analyzing the level of NDVI, we analyze its growth rate. Fig. 2 shows the annual growth rate of NDVI. The aggregation of the ten-day data for the period 1999–2010 results in 48 seasons (12 years × 4 seasons/year).

Interestingly, the growth rate fluctuates between +15% and −15% (see Fig. 2). Seasonal effects are visible but maybe not as clear-cut as one would have expected. Although it does hold that in winter the growth rate is usually negative, it is not always positive in spring. Fig. 3 presents the growth rate of NDVI for spring time only.

For the first half of the sample, there seems to be a two-year cycle: starting in 1999, the growth rate is positive, it then becomes negative, and in 2001, it is positive again. However, one should bear in mind that a negative growth rate does not imply that vegetation is not growing in spring. It merely states that in 2000 vegetation, growth was 4% less than in 1999. In other words, a "good" year is followed by a "bad" year, which is then followed by a "good" year again.

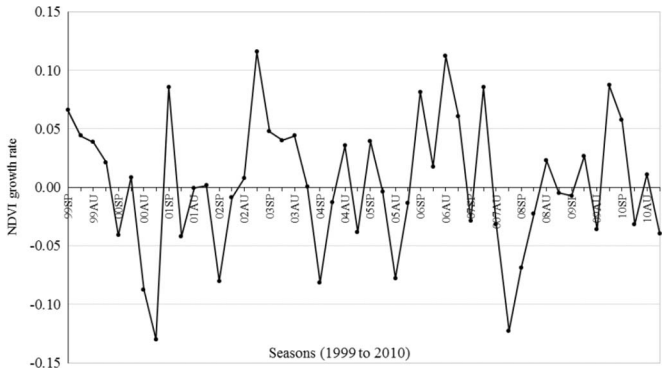

Fig. 2. Annual growth rate of NDVI for the period 1999–2000.

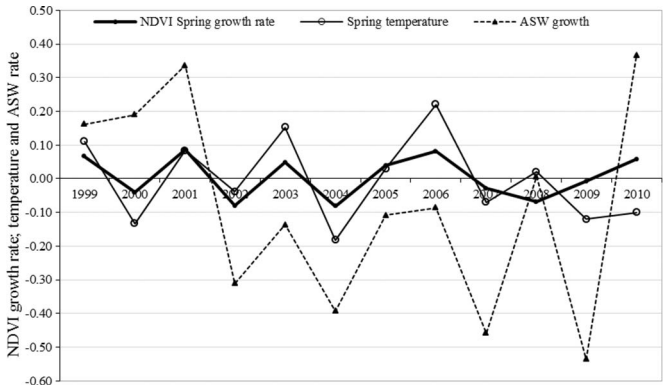

Fig. 3. Relationship between spring NDVI, temperature, and ASW growth rates for the period 1999–2010.

Importantly, from 2005 onward, the two-year cycle becomes a four-year cycle. Hence, a "good" year is followed by another good year, and this one is then followed by two "bad" years. It is worth noting that, at this stage, we cannot be sure whether this change of cycles implies a change of the temporal pattern or an irregular interannual variation. It is merely an observation without applying any statistical methods.

Remarkably, aggregation of the data reveals a symmetric behavior of the natural NDVI spring cycles as opposed to seasonal cycles. This refers to the amplitude (±8%) and the clear cyclic behavior, which also recently changed.

In the next step, we compare the spring NDVI cycles with the spring temperature cycles. A first indication of this link can be seen if we combine both growth rates of NDVI and temperature in one figure (see Fig. 3).

As in the case of the NDVI growth rate, there are two-year cycles visible up to 2007, where the cycle potentially becomes a four-year cycle. In difference to the NDVI growth rate, temperature variability is bigger. The temperature varies at some points in time (1999, 2005) by more than 15%.

The NDVI growth rate and the temperature growth rate behave in a cyclical way to each other until 2008. From 2008 onward, the link is different. In particular, for the years following 2008, it looks as if temperature and NDVI behave anticyclically with each other (see Fig. 3). Despite the obvious link of the two variables, it is remarkable that the higher fluctuation of temperature has only a reduced effect on the variability of the NDVI growth, if at all.

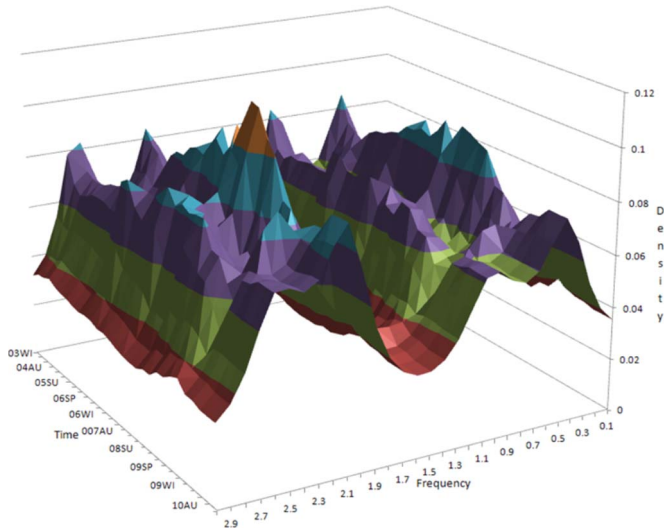

Fig. 4. Spectrum of the NDVI growth rate.

Last but not least, we also look at the growth rates of the spring NDVI and the ASW (see Fig. 3). The variability is higher than for the other two variables. The maximum is -50% in 2009. From 2001 to 2010, there is a two-year cycle visible, only once interrupted in 2005. Moreover, there also seems to be a nine-year cycle visible, namely, from 2001 to 2010.

Despite their different variability, both variables seem to move in line until 2008. As with the temperature, the relationship between NDVI and ASW should be positive.

In summary, these indicative results clearly show the existence of *natural* growth cycles. We discovered not only two-year cycles but also longer term cycles. Moreover, we could also see that the cycles are not constant. For the NDVI spring series, in particular, the two-year cycles seem to have changed to four-year cycles.

The variability of the three variables under consideration differs and so does their relationships.

The indicative results imply several issues: We need to detect which cycles are the most important one when we consider all seasons. We need a method that takes into account that cycles are not (necessarily) constant. Finally, we need a method that allows us to test the changing relationship between NDVI, soil water, and temperature.

For this reason, we decided to use a time–frequency approach that can tackle all the preceding issues. In what follows, we will shortly introduce time–frequency analysis before we apply it to the three variables.

B. Single Spectra of the NDVI Growth Rate

Fig. 4 shows the time-varying spectrum of the NDVI. The regression is based on all seasons rather than just the spring seasons, as shown earlier in this paper. For this reason, we should not necessarily expect the same cyclical behavior as in Fig. 3.

If the NDVI growth rate was a white noise process, then the spectrum would be completely flat. As one can see in Fig. 4, this is not the case. The spectrum shows peaks at the following frequencies: 0.5, 1, 2.1, and 2.5. Of these, the most important cycles are at the frequencies of 0.5 and 2.1. This corresponds to 12 and 3 seasons, respectively. The frequency of 1 corresponds to 6 seasons, and the frequency of 2.5 corresponds to 2.5 seasons.

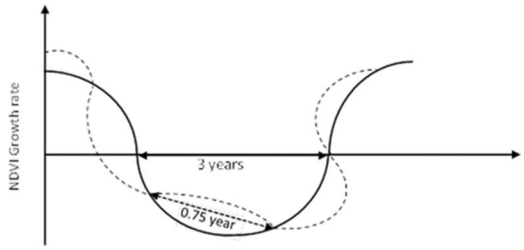

Fig. 5. Graphical interpretation of NDVI growth cycles. There are two fluctuations of equal strengths: one has a length of 3 years (solid line), and there is a shorter one of 0.75 year (dashed line).

In other words, the vegetation growth rate mainly follows 12- and 3-season cycles. Fig. 5 highlights the result.

In Fig. 5, the 12-season cycle represents 3 years and is the main cycle, whereas the 3-season cycle (or 0.75 years) fluctuates around the main cycle.

Table I shows the regression results for the series dlNDVI. This AR(8) model is the basis for the spectrum shown in Fig. 5. As one can see, the regression is robust as there is no autocorrelation. For the chosen model, this was, in fact, the lowest AIC value we could achieve. R^2 is relatively high with 99%, but there is also unexplained variance. Although the first four lags are statistically not significant at the end of the sample, they were at other sample points in time, which is why we kept them in the regression (see Table I). Hence, this table only shows the final regression for the last observation for reason of restricted space.

C. Cross-Spectra and Simulation Results

In the next step, we estimated the dependence of the NDVI growth rate on temperature and ASW rates according to (4) and (5). We used a bivariable approach in order to avoid potential multicollinearity. In other words, in the first regression, we estimated the dependence of the growth rate of NDVI on the growth rate of temperature, and in the second step, we estimated the dependence of the growth rate of NDVI on the growth rate of ASW. We start off with the temperature results.

Table II shows the regression results. As in the previous section, we only show the final observation results. All other results are available on request. The resulting coherence is shown in Fig. 6.

Fig. 6 shows that there are two cycles at which the link between the growth rate of NDVI and the temperature is biggest, namely, at frequencies of 0.8 and 2.4. These frequencies are very close to the original frequencies in Fig. 5. They correspond to cycles of 7.8 seasons (or 2 years) and 2.6 seasons (or three quarters of a year). The coherence close to these two cycles is very high as well. Thus, we can conclude that the temperature explains a lot of the spectrum apart from the short term (frequency of "π"), the long-run growth (frequency of "0"), and the cycle at a frequency of 1.6 (or 4 seasons, i.e., 1 year).

In order to analyze the NDVI-based growth rate sensitivity of the model, a number of simulations about changes in temperature and ASW were computed.

The regression results also allow us to look at the impact of a 10% change of the temperature on NDVI if everything else

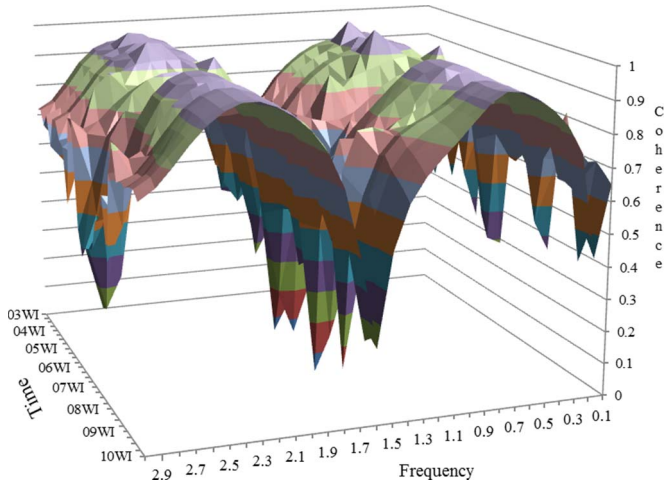

Fig. 6. Coherence between the growth rate of NDVI and the temperature.

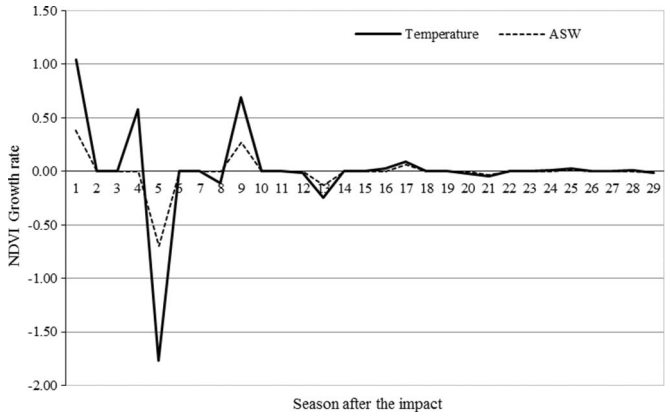

Fig. 7. Effects on the NDVI growth rate of a 10% change in the temperature and ASW growth rates.

remains constant. Fig. 7 assumes a 10% one-off increase in temperature and ASW.

Fig. 7 shows that most of the shock has been absorbed after 10 quarters, where the system returns to the steady state. From a time-series point of view, this indicates a stationary process, i.e., after a shock, the system returns to a steady-state value. It is worth noting that stationarity has not been imposed by the regression. It is the outcome of the regression, which could have been nonstationary as well.

It is interesting to note that the dynamics that are caused by a one-off increase in temperature by 10% imply positive and negative NDVI growth rates. The immediate effect of the increase in temperature is a 1% increase in the NDVI, which is followed by a 0.5% increase 4 seasons later. This increase is then completely removed in the following season, where the NDVI growth is reduced by 1.5%. These two-year cycles are in line with our observations made earlier in this paper. It is also important to note that the reaction of the NDVI growth rate to a change in temperature is underproportional to the change in temperature (about 10%).

Finally, we also analyze the impact of ASW on vegetation. We ask what NDVI growth cycles are determined by ASW. Fig. 8 gives the answer.

The coherence shown in Fig. 8 is based on the regression results in Table III. The coherence shows that the growth rate

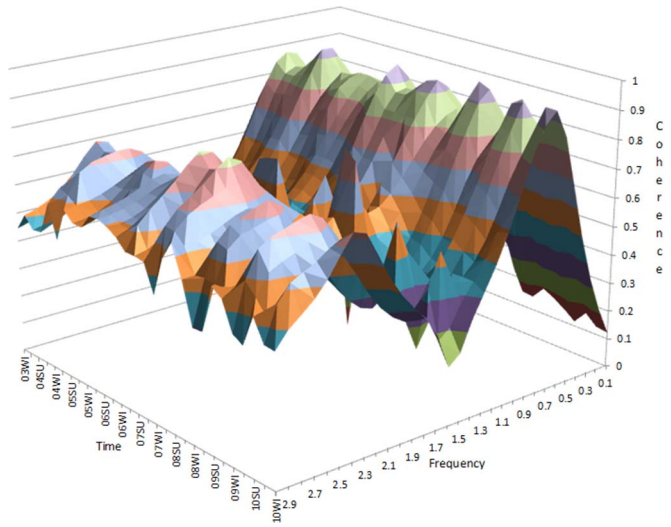

Fig. 8. Coherence between the growth rate of NDVI and the growth rate of ASW.

of the absorbed soil water explains 95% of the NDVI cycle at a frequency of 0.7, i.e., 9 seasons or 4.5 years. The second cycle the growth rate of ASW is explaining is at a frequency of 2.4 or 2.6 seasons. ASW explains about 50% of this cycle. This cycle closely corresponds to the cycle shown in Fig. 7, the spectrum of the NDVI growth rate. There is also coherence at a cycle of 1.3 of 0.5 years, but this coherence diminishes over time. The two main coherences stay important throughout the sample, although the long-run cycle coherence has slightly increased toward the end of the sample.

Overall, the mass of the spectrum, which the growth rate of ASW is explaining, is less than the temperature. Given an R^2 of 0.95, this highlights that time-series results alone may sometimes be misleading: One may not capture the crucial cycles if one only takes into account time-series properties. This is not to say that time-series results are wrong; one just has to be careful on interpreting them.

Like in the case of the temperature, we can also investigate the effects of a 10% increase in the ASW (see Fig. 7).

In Fig. 7, we can see that a 10% change in the growth rate of ASW leads to a 0.4% change in the growth rate of NDVI. Like in the case of the temperature, most adjustments have been finished after 10 seasons. Given that the behavior of the system is very similar to the temperature shock, this supports the hypothesis that a particular area can only support a certain vegetation level. From this point of view, it is certainly no coincidence that, like in the case of temperature, after 5 seasons, there is a negative effect on NDVI by about 0.6%, which is balanced four seasons later. Overall, the impact of a 10% on the NDVI growth rate is close to zero after the system returns to the steady state.

V. Discussion

The increased importance of satellite data in support of research in impact of climate on the vegetation dynamics leads to a strong need for a more comprehensive understanding of time-series changes. We apply a time–frequency approach, which not only gives us the cyclical properties but also gives how they changed over time. This alternative approach was partially

presented in previous work of Cunha and Richter [41] and Hughes Hallett and Richter [37], [40].

We achieved all of the results by estimating a dynamic time-series model. The time-series model is characterized by its lag polynomials and the time-varying weights. The lag polynomial allows us to describe the dynamic properties of the estimated relationships. As the lag polynomial is time varying itself, the Fourier transform becomes time varying. As a result, we have a time-varying spectrum and a time-varying coherence. In traditional frequency-domain analysis, a time series has to be stationary for the frequency estimators to be unbiased. By using a time-varying estimator, the series does not have to be stationary anymore as long as the nonstationarity was caused by structural breaks of which the Kalman filter is able to take care of. Therefore, with this approach, we gain more insights in the dynamic properties of a system than with the more "common" approaches (see Section I).

The results of the satellite-based grassland growth rate clearly show the existence of not only two-year spring cycles but also longer term cycles (see Figs. 2 and 3). Moreover, these cycles are not constant. In particular, the two-year cycles have changed to four-year cycles. However, if we look at the cyclical behavior of all seasons, a change of the cyclical behavior could not be observed (see Fig. 4). As a result, it seems that individual seasons may undergo cyclical changes that are offset by other seasons. This area therefore needs further research.

Our results also stated that temperature and ASW are important drivers of vegetation growth rate cycles. The variability of the three variables under consideration differs and so does their relationships. However, the link between satellite-derived vegetation growth rate and temperature is positive, as well as the link between vegetation growth rate and ASW.

We can also recognize a relative increase in importance of soil water at constant importance of temperature (see Fig. 7). Despite soil water explaining about 50% of short-term cycles, temperature still explains about 90% of those cycles. Because evapotranspiration rates are positively related to temperature, increased temperatures are likely to be associated with increased rates of soil water loss. Therefore, if temperature warms without a compensating increase in precipitation, plants may become increasingly water stressed, which could lead to decreases in growth rate where the irrigation was not possible.

The individual shocks of the temperature and ASW to the system have similar dynamic effects/consequences (see Fig. 7).

The question is what drives this behavior? Why is the growth rate of the NDVI stationary? It seems that a particular area can only support a certain vegetation level. A shock to this system can therefore only have a temporary effect, but not a permanent one, unless all other determinants of vegetation growth will support an increased vegetation, which in this scenario/regression they do not do (all other variables stayed the same). As a result, an increase in vegetation has to be offset later. The estimation results show that this offsetting starts a year later. This was not imposed in the regression and is purely a regression result. It also indicates that a shock to the system causes a two-year cycle: in the first year, vegetation increases; in the second year, it decreases.

The perennial nature of grasslands and the extensive management of soil nutrient cycles (no fertilizers added) means that soil organic matter (SOM) is a main source of soil nutrients, and thus, carry effects from year to year should be expected. Our study also shows that grass growth rates depend both on the immediate impact of the spring temperature and on the spring temperature from the previous year. As such, we hypothesize that the SOM dynamics and nitrogen cycle are intimately coupled, and temperature in mountain meadows colimits this process so that it extends for several years.

The results support the hypothesis that vegetation dynamics are physiologically dependent in several ways on the previous years. Therefore, a time-varying spectral approach, capable of separating out changes at different cyclical frequencies and points in time with respect to grassland growth, will need to provide the flexibility to capture these features and the important ecophysiological information contained therein.

VI. Conclusion

We have modeled cyclical satellite-based grassland growth rate with a time–frequency approach. It provides the cyclical properties of the satellite-based growth rate and what cycles, in particular, are explained by the climate variables.

The cyclical analysis revealed that there are more than just seasonal cycles working for the NDVI-based vegetation growth. We could show that the cyclical properties of NDVI are not constant over time.

While this time–frequency approach of satellite-based vegetation growth cycles can only give indications of causal relationships on potential climatic growth impact, they provide the catalyst for causal hypothesis generation, namely, for the plant–soil interactions, which could be tested where other data sources are available. The quantification of the relative impact of these myriad factors on the grassland dynamics is still a huge challenge for developing strategies for the sustainable use of grassland resources in northeast Portugal, as well as other extensively managed grassland systems worldwide.

Acknowledgment

The authors would like to thank the VEGETATION program for providing the satellite images. Work financed by European Regional Development Fund (ERDF), programme COMPETE and National funds by FCT-Fundação para a Ciência e a Tecnologia, project FCT EXPL/AGR-PRO/1559/2012.

References

[1] B. Boashash and A. Reilly, *Algorithms for Time–Frequency Signal Analysis*. Melbourne, Australia: Longman Cheshire, 1992, pp. 163–181.

[2] J. P. Theurillat and A. Guisan, "Potential impact of climate change on vegetation in the European Alps: A review," *Clim. Change*, vol. 50, no. 1/2, pp. 77–109, Jul. 2001.

[3] H. F. Diaz, M. Grosjean, and L. Graumlich, "Climate variability and change in high elevation regions: Past, present and future," *Clim. Change*, vol. 59, no. 1/2, pp. 1–4, Jul. 2003.

[4] M. E. Assessment, *Ecosystem and Human Wellbeing: Policy Responses*. Washington, DC, USA: Island Press, 2005.

[5] L. Telesca and R. Lasaponara, "Quantifying intra-annual persistent behaviour in SPOT_VEGETATION NDVI data for Mediterranean ecosystems of southern Italy," *Remote Sens. Environ.*, vol. 101, no. 1, pp. 95–103, Mar. 2006.

[6] P. Cayrol, A. Chehbouni, L. Kergoat, G. Dedieu, P. Mordelet, and Y. Nouvellon, "Grassland modeling and monitoring with SPOT-4 VEGETATION instrument during the 1997–1999 SALSA experiment," *Agricultural Forest Meteorol.*, vol. 105, no. 1–3, pp. 91–115, Nov. 2000.

[7] M. Cunha, A. Marcal, and L. Silva, "Very early prediction of wine yield based on satellite data from VEGETATION," *Int. J. Remote Sens.*, vol. 31, no. 12, pp. 3125–3142, Apr. 2010.
[8] I. Poças, M. Cunha, and L. Pereira, "Dynamics of semi-natural grassland meadows inferred from SPOT-Vegetation and field spectroradiometer data," *Int. J. Remote Sens.*, vol. 33, no. 14, pp. 4334–4355, Jul. 2012.
[9] M. Cunha, I. Pocas, A. R. S. Marcal, A. Rodrigues, and L. S. Pereira, "Evaluating MODIS vegetation indices using ground based measurements in mountain semi-natural meadows of northeast Portugal," *Proc. IEEE IGARSS*, pp. 1525–1528, 2010.
[10] A. Rodrigues, A. R. Marcal, and M. Cunha, "Monitoring vegetation dynamics inferred by satellite data using the PhenoSat tool," *IEEE Trans. Geosci. Remote Sens.*, vol. 51, no. 44, pp. 2096–2104, Apr. 2013.
[11] E. F. Lambin and A. H. Strahler, "Change-vector analysis in multitemporal space—A tool to detect and categorize land-cover change processes using high temporal-resolution satellite data," *Remote Sens. Environ.*, vol. 48, no. 2, pp. 231–244, May 1994.
[12] J. L. Lovell and R. D. Graetz, "Filtering pathfinder AVHRR land NDVI data for Australia," *Int. J. Remote Sens.*, vol. 22, no. 13, pp. 2649–2654, Sep. 2001.
[13] B. C. Reed, M. White, and J. F. Brown, "Remote sensing phenology," in *Phenology: An Integrative Environmental Science*. Dordrecht, The Netherlands: Kluwer, 2003, pp. 365–381.
[14] X. Y. Zhang, M. A. Friedl, C. B. Schaaf, A. H. Strahler, J. C. F. Hodges, F. Gao, B. C. Reed, and A. Huete, "Monitoring vegetation phenology using MODIS," *Remote Sens. Environ.*, vol. 84, no. 3, pp. 471–475, Mar. 2003.
[15] P. Jonsson and L. Eklundh, "TIMESAT—A program for analyzing time-series of satellite sensor data," *Comput. Geosci.*, vol. 30, no. 8, pp. 833–845, Oct. 2004.
[16] J. Chen, P. Jonsson, M. Tamura, Z. H. Gu, B. Matsushita, and L. Eklundh, "A simple method for reconstructing a high-quality NDVI time-series data set based on the Savitzky–Golay filter," *Remote Sens. Environ.*, vol. 91, no. 3/4, pp. 332–344, Jun. 2004.
[17] T. Sakamoto, M. Yokozawa, H. Toritani, M. Shibayama, N. Ishitsuka, and H. Ohno, "A crop phenology detection method using time-series MODIS data," *Remote Sens. Environ.*, vol. 96, no. 3/4, pp. 366–374, Jun. 2005.
[18] J. F. Hermance, R. W. Jacob, B. A. Bradley, and J. F. Mustard, "Extracting phenological signals from multiyear AVHRR NDVI time series: Framework for applying high-order annual splines with roughness damping," *IEEE Trans. Geosci. Remote Sens.*, vol. 45, no. 10, pp. 3264–3276, Oct. 2007.
[19] B. A. Bradley, R. W. Jacob, J. F. Hermance, and J. F. Mustard, "A curve fitting procedure to derive inter-annual phenologies from time series of noisy satellite NDVI data," *Remote Sens. Environ.*, vol. 106, no. 2, pp. 137–145, Jan. 2007.
[20] J. Verbesselt, R. Hyndman, A. Zeileis, and D. Culvenor, "Phenological change detection while accounting for abrupt and gradual trends in satellite image time series," *Remote Sens. Environ.*, vol. 114, no. 12, pp. 2970–2980, Dec. 2010.
[21] C. Atzberger and P. H. C. Eilers, "Evaluating the effectiveness of smoothing algorithms in the absence of ground reference measurements," *Int. J. Remote Sens.*, vol. 32, no. 13, pp. 3689–3709, 2011.
[22] W. Q. Zhu, Y. Z. Pan, H. He, L. L. Wang, M. J. Mou, and J. H. Liu, "A changing-weight filter method for reconstructing a high-quality NDVI time series to preserve the integrity of vegetation phenology," *IEEE Trans. Geosci. Remote Sens.*, vol. 50, no. 4, pp. 1085–1094, Apr. 2012.
[23] A. Moody and D. M. Johnson, "Land-surface phenologies from AVHRR using the discrete Fourier transform," *Remote Sens. Environ.*, vol. 75, no. 3, pp. 305–323, Mar. 2001.
[24] S. Lhermitte, J. VerBesselt, W. W. Verstraeten, and P. Coppin, "A comparison of time series similarity measures for classification and change detection of ecosystem dynamics," *Remote Sens. Environ.*, vol. 115, no. 12, pp. 3129–3152, Dec. 2011.
[25] J. N. Hird and G. J. McDermid, "Noise reduction of NDVI time series: An empirical comparison of selected techniques," *Remote Sens. Environ.*, vol. 113, no. 1, pp. 248–258, Jan. 2009.
[26] P. Coppin, I. Jonckheere, K. Nackaerts, B. Muys, and E. Lambin, "Digital change detection methods in ecosystem monitoring: A review," *Int. J. Remote Sens.*, vol. 25, no. 9, pp. 1565–1596, May 2004.
[27] J. Wang, J. J. Meng, and Y. L. Cai, "Assessing vegetation dynamics impacted by climate change in the southwestern karst region of China with AVHRR NDVI and AVHRR NPP time-series," *Environ. Geol.*, vol. 54, no. 6, pp. 1185–1195, May 2008.
[28] C. Thornthwaite and J. Mather, *The Water Balance*. Centerton, NJ, USA: Drexel Inst. Technol., Lab. Climatol., 1955.
[29] *Free VEGETATION Products*, VITO, Mol, Belgium, Nov. 5, 2011.
[30] W. H. Greene, *Econometric Analysis*. Upper Saddle River, NJ, USA: Prentice-Hall, 1997.
[31] M. Stone, "Comments on model selection criteria of Akaike and Schwarz," *J. R. Stat. Soc., Ser. B (Methodological)*, vol. 41, no. 2, pp. 276–278, 1979.
[32] W. Ploberger, W. Krämer, and K. Kontrus, "A new test for structural stability in the linear regression model," *J. Econom.*, vol. 40, no. 2, pp. 307–318, Feb. 1989.
[33] L. R. LaMotte and A. J. McWorther, "An exact test for the presence of random walk coefficients in a linear regression," *J. Amer. Stat. Assoc.*, vol. 73, no. 364, pp. 816–820, 1978.
[34] D. Gabor, "Theory of communication," *J. Inst. Elect. Eng.*, vol. 93, no. 26, pp. 429–457, Nov. 1946.
[35] Z. Lin, "An introduction to time–frequency signal analysis," *Sens. Rev.*, vol. 17, no. 1, pp. 46–53, 1997.
[36] A. Hughes Hallett and C. Richter, "Is the US no longer the economy of first resort? Changing economic relationships in the Asia–Pacific Region," *Int. Econom. Econom. Policy*, vol. 6, no. 2, pp. 207–234, Jul. 2009.
[37] A. Hughes Hallett and C. Richter, "Has there been any structural convergence in the transmission of European monetary policies?" *Int. Econom. Econom. Policy*, vol. 6, no. 2, pp. 85–101, Jul. 2009.
[38] A. Hughes Hallett and C. Richter, "Economics in the backyard: How much convergence is there between China and her special regions?" *World Econom.*, vol. 32, no. 6, pp. 819–861, Jun. 2009.
[39] J. Wolters, *Stochastic Dynamic Properties of Linear Econometric Models*. Berlin, Germany: Springer-Verlag, 1980.
[40] A. Hughes Hallett and C. Richter, "Is the convergence of business cycles a global or regional issue? The UK, US and Euroland," *J. Int. Finance Econom.*, vol. 11, no. 3, pp. 177–194, Jul. 2006.
[41] M. Cunha and C. Richter, "Measuring the impact of temperature changes on the wine production in the Douro region using the short time Fourier transform," *Int. J. Biometeorol.*, vol. 56, no. 2, pp. 357–370, Mar. 2012.

Mario Cunha was born in Grimancelos (Barcelos), Portugal. He received the M.Sc. degree in agronomic engineering from Universidade de Trás-os-Montes e Alto Douro, Villa Real, Portugal, and the Ph.D. degree in agrarian sciences from Universidade do Porto, Porto, Portugal.

He is currently an Assistant Professor with the Department of Geosciences, Environment and Spatial Planning, Faculdade de Ciências, Universidade do Porto. His research interests include various topics in remote sensing applications, agronomy, agricultural engineering, and bioclimatic environment.

Dr. Cunha was the recipient of the Syngenta Crop Protection Innovation in Agriculture Award in 2007.

Christian Richter received the Ph.D. degree in economics in 2001.

He is currently a Principal Lecturer in transnational education, economics, and management with the University of Bedfordshire, Bedfordshire, U.K. His main areas of research are behavioral economics and finance, convergence of business cycles, eurozone crisis, financial economics, time frequency analysis, and climate change.

Dr. Richter is an Honorary Chair of the International Network for Economic Research. He is an editorial board member of many scientific journals. He was a recipient of a merit award from Kingston University in 2009. He won research grants from The Leverhulme Trust and the Austrian Central Bank.

A Time–Frequency Analysis on the Impact of Climate Variability on Semi-Natural Mountain Meadows

Mario Cunha and Christian Richter

***Abstract*—This paper analyzes the impact of climate dynamics on vegetation growth for a rural mountainous region in northeastern Portugal. As a measure of vegetation growth, we use the normalized difference vegetation index (NDVI), which is based on the ten-day synthesis data set (S10) from Satellite Pour l'Observation de la Terre (SPOT-VEGETATION) imagery from 1998 to 2011. We test whether the dynamic growth pattern of the NDVI has changed due to climate variability, and we test the relationship of NDVI with temperature and available soil water (ASW). In order to do so, we use a time–frequency approach based on Kalman filter regressions in the time domain. The advantage of our approach is that it can be used even in the case where the sample size is relatively small. By estimating the important relationships in the time domain first and transferring them into the frequency domain, we are still able to derive a complete spectrum over all frequencies. In our example, we find a change of the cyclical pattern for the spring season and different changes if we take into account all seasons. In other words, we can distinguish between deterministic changes of the vegetation cycles and stochastic changes that only occur randomly. Deterministic changes imply that the data-generating process has changed (such as climate), whereas stochastic changes imply only temporary changes. We find that individual seasons undergo cyclical changes that are different from other seasons. Moreover, our analysis shows that temperature and ASW are the main drivers of vegetation growth. We can also recognize a shift of the relative importance away from temperature to soil water.**

***Index Terms*—Climate variability, Kalman filter, mountain meadows, normalized difference vegetation index (NDVI), time-varying spectra, vegetation dynamics.**

I. Introduction

TIME–frequency analysis is used in engineering for quite some time [1]. Time–frequency analysis investigates cycles whose properties may change over time. The inspiration for this paper is therefore to investigate whether climate change has a (changing) impact on natural growth cycles. Climate changes are particularly serious for mountainous regions because they are among the most fragile environments in the world [2], [3] and are recognized as the key supporting ecosystem service related to natural resources conservation, as defined by the Millennium Ecosystem Assessment [4]. Therefore, if climate change has an impact on growth cycles, it should be measurable in a sensitive system such as mountainous regions. As an example, we study the mountainous grassland system in northeast Portugal. The traditional landscape of the mountainous region of northeastern Portugal is characterized by the ancestral agropastoral or grassland system extensively used for hay and grazing. The increased water constrains due to sectorial competition for water uses and the foreseeable climate warming endangers the sustainability of these lameiros. Hence, our results may be also used for conservation strategies to preserve these meadows.

Remote sensing of vegetation dynamics at regional and field scales is often pursued using high-temporal-resolution sensors [advanced very high resolution radiometer, medium resolution imaging spectrometer, moderate resolution imaging spectroradiometer, and Satellite Pour l'Observation de la Terre (SPOT-VEGETATION)]. The data received from these sensors provide large area coverage with high frequency, limited only by the compositing period needed to remove the effects of clouds and cloud shadow [5]–[7]. Results from previous works show that the normalized difference vegetation index (NDVI) profile provided by the VEGETATION sensor, on board the most recent SPOT—SPOT_VGT—fits well the characteristics of vegetation growth dynamics and associated management practices in the semi-natural meadows of the mountainous region of northeast Portugal [8]–[10]. Hence, in this paper, we use the NDVI time series based on SPOT_VGT sensor imagery to infer about the impact of climate on these semi-natural meadows and to model vegetation dynamics.

Several approaches based on temporal trajectory analysis have been proposed for smoothing and detecting temporal changes in vegetation dynamics such as change vector analysis [11], Best Index Slope Extraction [12], moving averages [13], double logistic model [14], asymmetric Gaussian [15], sliding windows [16], wavelet decomposition [17], harmonic series and higher order splines [18], [19], Breaks For additive Seasonal and Trend [20], Whittaker smoother [21], changing-weight filter [22], discrete Fourier transform [23], and frequency analysis [24]. Many of these techniques need complementary complicate and tedious tests (e.g., derivatives, specific threshold, or change trajectories) to extract the time-series changes. Reviews of the merits and limitations of these techniques can be found in [18], [21], [22], and [24]–[26]. According to this literature, stationarity assumptions, data quality, sensor noise, and complications of the methods can make it challenging to quantify the separate sources of information that influence the signal and

Manuscript received January 9, 2013; revised June 19, 2013 and November 2, 2013; accepted November 23, 2013.

M. Cunha is with the Centro de Investigação em Ciências Geo-Espaciais, Faculdade de Ciências, Universidade do Porto, 4485-661 Vairão, Portugal (e-mail: mcunha@mail.icav.up.pt).

C. Richter is with the University of Bedfordshire Business School, University of Bedfordshire, Bedfordshire LU1 3JU, U.K. (e-mail: Christian.Richter@beds.ac.uk).

Color versions of one or more of the figures in this paper are available online at http://ieeexplore.ieee.org.

Digital Object Identifier 10.1109/TGRS.2013.2295321

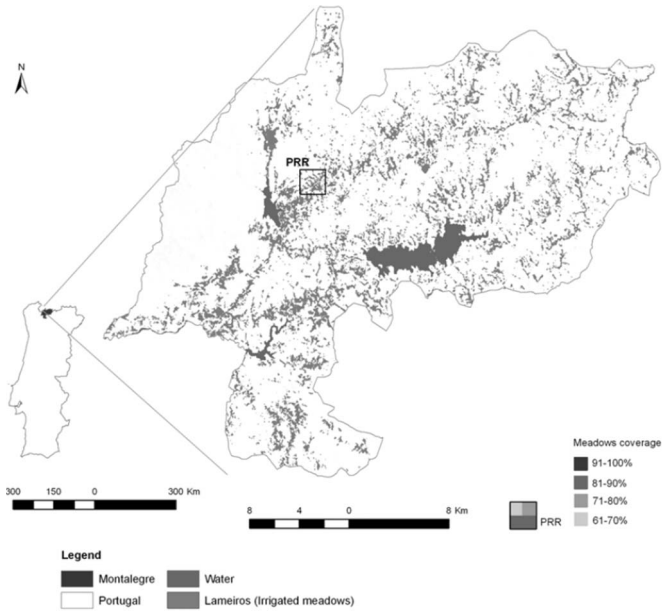

Fig. 1. Location of the study area (Montalegre) in northeast Portugal and the test site located in PRR, showing the meadow coverage in Montalegre (in gray). The PRR (2×2 pixels) coordinates (Datum WGS84) of the upper left site corner are $7°55'04$ W and $41°48'32''$ N. Details of meadow coverage per pixel in the test site are also given as percentages.

to determine what constitutes a significant change. Moreover, the frequently used time-series analysis of satellite derived vegetation growth data (e.g., [8], [27]) are not capable to integrate and quantify the seasonal and interannual impacts of climate on vegetation dynamics.

It is well known that vegetation dynamics depend on the climate. However, an open question is how sensitive are seasonal and interannual cycles to climate variability. Therefore, a time-varying spectral approach, which is capable of separating out changes at different cyclical frequencies (including trend) in the grassland growth, is needed to provide the flexibility to capture these features.

We identify the importance of variability of climate for cyclical properties in the satellite-based grassland growth rate and consider how the impacts of these events may be predicted. The following section describes the test site and the methods used to derive the data. Section III briefly explains the statistical methods used in this paper. Section IV gives the results. A discussion is provided in Section V, and Section VI concludes this paper.

II. Materials and Methods

A. Study Area

The region of analysis covers a large area of the mountainous region of Montalegre, northeast Portugal (see Fig. 1).

The large pixel size of SPOT_VGT images (1 km) determines the criteria for selection of the test site, which have to include large contiguous areas with lameiros fields. Therefore, one suitable test site was selected in Montalegre municipality, location of Paredes do Rio (PRR). The test sites have 2×2 pixels (of 1×1 km), in a compact group of contiguous pixels, all with 65% or more lameiros coverage. The average lameiros coverage occupancy of the PRR test site is 77.8% (see Fig. 1).

These meadows are conveniently located in areas of high water availability, loamy soils, and over 700–800 m high. In this region, the Atlantic climate favors high precipitation occurrence (1531 mm/year), mainly occurring from autumn to spring, autumn–winter temperatures lower than 12 °C. and mean monthly temperatures ranging from 3.5 °C to 17.2 °C.

B. Meteorological Data and Soil Water Balance

We use meteorological observations for the years 1998 to 2011 from the weather station of Montalegre ($41°49'$ N : $7°47'$ W: 1005 m above sea level) located in the proximity of the test site. The meteorological data consist of daily observations of temperature (maximum and minimum) and precipitation. These general meteorological parameters are used to derive other variables: mean temperature (Tm, °C), potential evapotranspiration (ETP, mm), and other variables related to soil water balance.

The Thornthwaite–Matter (T–M) [28] mass conservation climatic water budget model is then performed to simulate ten-day soil water balance. Dekadal ETP is estimated using the empirical Thornthwaite equation that relies on mean temperature and average day length (in hours per day). The T–M model tracks the soil water through time by balancing the inputs (precipitation) and outputs of water (ETP). The soil operates as a "bucket" with a user-defined field available water capacity: 100 mm in this study. The ability to remove soil moisture has been set to decrease exponentially with the decreasing soil-moisture content. The model output includes available soil water (ASW) that ranges from 0 to 100 mm. This methodology was chosen because of its simplicity and small quantity of input meteorological data needed.

C. Satellite Data

In this paper, we use the satellite imagery provided by SPOT_VGT for the period 1998 (April) to 2011 (March) to examine the dynamic patterns of grassland grow inferred by the NDVI. This satellite has an intermediate spatial resolution (1 km), and the images are corrected for radiometric, geometric, and atmospheric effects. Ten-day composite VEGETATION products (S10) are obtained from the compilation of daily data. In the SPOT_VGT S10 composites, the resulting surface reflectance value for each pixel corresponds to the date with the maximum NDVI reflectance at the top of the atmosphere for that pixel [29].

The pixels of the test site (2×2 pixels) were averaged to create the NDVI value for each time period. This was done to prevent misregistration and errors from other sources; these errors could contaminate the temporal profiles.

The NDVI is a variable that is truncated (it can only adopt values between -1 and 1). In a truncated sample, information on the regressors is available only if the regressand is actually observed. In our example, we cannot observe values of the NDVI below -1 and above 1 (may be seen as a truncated distribution), which results in a nonnomal distribution [30]. This implies that either one has to adopt an estimation technique that takes truncated variables into account or we have to transform NDVI data into a nontruncated variable. For this reason, we transformed NDVI into a growth rate. This growth rate is not truncated anymore; thus, common estimation techniques can be used. Given our data set, we can construct different growth

rates. We have tested these different growth rates such as ten-day growth rates and monthly growth rates, but we found that the model using the annual growth rate was statistically superior to all other models in the sense that it minimized the Akaike and Schwartz information criteria [31]. We calculated the annual growth rate in the following way: we first calculated for all observations of NDVI the annual growth rate. In accordance with the seasonal calendar, we then calculated the average annual growth rate for a particular season. Therefore, in this paper, we work with average data on seasonal level, and we use annual growth rates rather than level values.

To make the approach consistent, we also use the same growth rates for temperature and soil water. Hence, in all regressions to come, all variables refer to the same time period and have the same dimension, namely, percent.

III. Time–Frequency Analysis of the NDVI

A. First Step: Estimation in the Time Domain

In contrast to "common" frequency approaches, we do not estimate the spectrum directly. The reason is that this usually requires a large number of observations. If one takes into account nonstationary spectra as well, then the number of necessary observations increases even more. By estimating a time-series model, first, we avoid this problem. Moreover, an important advantage of our approach is that we can *calculate* a spectrum showing *all* frequencies (even the long ones) with a relatively small sample size. We can further test whether the properties of the long cycles may have changed over the sample period. Thus, our conclusions concerning the long-run (and short-run) cycle properties are only valid for the sample under consideration and may change afterward or have been different before our sample. The crucial point is, however, that we can infer from small-sample long-run cycle properties.

In the first step, we estimate the cyclic behavior of the growth rate of each individual variable, i.e., NDVI, ASW, and Tm. In order to do so, we have to estimate an autoregressive model of order p, i.e., AR(p), where p is determined by statistical tests. In order to allow for the possible changes in the parameters, we will employ a time-varying model AR(p) by applying a Kalman filter to the chosen model as follows:

$$y_t = \alpha_{0,t} + \sum_{i=1}^{9} \alpha_{i,t} y_{t-i} + \varepsilon_t \tag{1}$$

where y_t is the NDVI growth rate, and

$$\alpha_{i,t} = \alpha_{i,t-1} + \eta_{i,t}, \qquad \text{for } i = 0, \ldots, 9 \tag{2}$$

and $\varepsilon_t, \eta_{i,t} \sim$ i.i.d.$(0, \sigma^2_{\varepsilon,\eta_i})$, for $i = 0, \ldots, 9$.

α_s are the unknown coefficients to be estimated. We employ a general to specific approach (starting with $p = 9$) to obtain a final specification for (1), eliminating insignificant lags. The maximum number of lags was determined by the Akaike information criterion (AIC). For each regression, we applied a set of diagnostic tests, as shown in Tables I–III, to confirm the final specification found.

Using the aforementioned specification implies that we get a set of parameter values for each point in time (here, a point in time is one season). Hence, a particular parameter could be significant for all points in time or at some periods but not others, or it might never be significant. These parameter changes are at the heart of this paper as they imply changes in the lag structure and, hence, changes in the spectral results. If

TABLE I
Regression Results for *dl*NDVI

Estimation by Kalman Filter			
Dependent Variable	dlNDVI		
Usable Observations	48	Degrees of Freedom	45
R2	0.99308		
Mean of Dep.Variable	0.00356	Std Error of dep. variable	0.054619
Standard Error of Estimate	0.051779	SS Residuals	0.093837
Akaike Information Criterion	0.06117	Ljung-Box Test: Q*(9) =	13.3008
Variable	Coeff	Std Error	T-Stat
Constant	-0.0113	0.0441	-0.2559
dlNDVI {3}	0.1260	0.0330	3.8128
dlNDVI {4}	-0.4198	0.0641	-6.5492
dlNDVI {8}	-0.2358	0.0706	-3.3410

Annual growth rate of NDVI (dlNDVI)

TABLE II
Regression Results Between *dl*NDVI and Temperature

Estimation by Kalman Filter			
Dependent Variable	dlNDVI		
Usable Observations	48	Degrees of Freedom	42
R2	0.97282		
Mean of Dependent Variable	0.0036	Std Error of dep. variable	0.0546
Standard Error of Estimate	0.0779	Sum of Squared Residuals	0.1943
Akaike Information Criterion	0.1043	Ljung-Box Test: Q*(9) =	16.4616.
Variable	Coeff	Std Error	T-Stat
Constant	-0.0116	0.0352	-0.3305
dlNDVI {4}	-0.7842	0.0925	-8.4767
dlNDVI {8}	-0.1021	0.0400	-2.5526
dlTmed	0.0863	0.0182	4.7353
dlTmed {3}	0.0978	0.0210	4.6718
dtTmed {4}	-0.1112	0.0305	-3.6415
dlTmed {7}	-0.0823	0.0228	-3.6076

Annual growth rate of NDVI (dlNDVI)

TABLE III
Regression Results Between *dl*NDVI and ASW

Estimation by Kalman Filter			
Dependent Variable	dlNDVI		
Usable Observations	48	Degrees of Freedom	42
R2	0.97282		
Mean of Dependent Variable	0.0036	Std Error of dep. variable	0.0546
Standard Error of Estimate	0.0779	Sum of Squared Residuals	0.1943
Akaike Information Criterion	0.1043	Ljung-Box Test: Q*(9) =	16.4616.
Variable	Coeff	Std Error	T-Stat
Constant	-0.0116	0.0352	-0.3305
dlNDVI {4}	-0.7842	0.0925	-8.4767
dlNDVI {8}	-0.1021	0.0400	-2.5526
dlTmed	0.0863	0.0182	4.7353
dlTmed {3}	0.0978	0.0210	4.6718
dtTmed {4}	-0.1112	0.0305	-3.6415
dlTmed {7}	-0.0823	0.0228	-3.6076

Annual growth rate of NDVI (dlNDVI)

a parameter was significant for some periods but not others, it was kept in the equation with a parameter value of zero for those periods in which it was insignificant. This strategy minimized the AIC and led to a parsimonious specification. Finally, we tested the residuals in each regression for autocorrelation and heteroscedasticity.

The final specification [see (1) and (2)] was then *validated* using two different stability tests. The first is the fluctuation test in Ploberger *et al.* [32], which detects *discrete* breaks at any point in time in the coefficients of a (possibly dynamic) regression. The second test is due to LaMotte and McWorther [33] and is specifically designed to detect *random* parameter variation of a specific unit root form (our specification). We found that the random walk hypothesis for the parameters was justified for each model (results available on request). We also test for autocorrelation of the residuals. For this purpose, we use the Ljung–Box test, which allows for autocorrelated residuals of order p. In all our regressions, we could reject the hypothesis of autocorrelation.

It should be noted that all our tests of significance and significant differences in parameters are being conducted in the time domain *before* transferring to the frequency domain. This is because no statistical tests exist for calculated spectra (the data transformations are nonlinear and involve complex arithmetic). Stability tests are important here because our spectra are sensitive to changes in the underlying parameters. However, given the extensive stability and specification tests conducted, we know there is no reason to switch to another model that fails to pass those tests.

Once this regression is done, it gives us a time-varying AR(p) model. From this AR(p) we can then *calculate* the short–time Fourier transform as outlined below, and as originally suggested by Gabor [34], in order to *calculate* the associated time-varying spectrum.

B. Second Step: Spectrum Analysis

Having estimated the time-series model, we are now able to analyze the power spectral density (PSD) function of the growth rate of NDVI. The PSD function shows the strength of the variations (energy) of a time series at each frequency of oscillation. In the diagram, it shows at which frequency variations are strong/powerful and at which frequencies the variations are weak (expressed in "energy"). The unit of measurement in the PSD is energy (variance) per frequency, frequency band, or cycle length.

In order to calculate the spectrum from an estimated representation of (1), we use the fast Fourier transform (FFT). Using the FFT, the time-varying spectrum of the growth rate series can be calculated as follows [35]:

$$P_t(\omega) = \frac{\sigma^2}{\left|1 + \sum_{i=1}^{9} \alpha_{i,t} \exp(-j\omega i)\right|_t^2} \tag{3}$$

where ω is the angular frequency, and j is a complex number. The main advantage of this method is that, at any point in time, a power spectrum can be instantaneously calculated from the updated parameters of the model. Hence, we are able to generate a power spectrum even if we have a short time series and even if that time series contains structural breaks.

C. Third Step: Cross-Spectrum Analysis

In this paper, we also investigate the linkage between different NDVI-based vegetation growth cycles. In the frequency domain, the natural tool to do that is the coherence.

Suppose now we are interested in the relationship between two variables $\{y_t\}$ and $\{x_t\}$, where $\{y_t\}$ is the grass growth rate and $\{x_t\}$ is the temperature variability, for example. We can then estimate an autoregressive distributed lag model (ARDL(p, q) of the order (p, q), where p gives the number of lags of the endogenous variable and q gives the number of lags of the exogenous variable. Using the lag polynomial, we can write the (ARDL(p, q) model in general terms as follows:

$$V(L)_t y_t = A(L)_t x_t + u_t, u_t \sim \text{i.i.d.}(0, \sigma^2) \tag{4}$$

where $A(L)_t$ and $V(L)_t$ are filters, and L is the lag operator such that $\text{L}z_t = z_{t-1}$. Notice that the lag structures $A(L)_t$ and $V(L)_t$ are time varying. That means we need to use a state-space model (we use the Kalman filter again) to estimate the implied lag structure. That is

$$\begin{aligned} v_{i,t} &= v_{i,t-1} + \varepsilon_{i,t}, \text{ for } i = 1, \ldots, p \text{ and } \varepsilon_{i,t} \sim \left(0, \sigma^2_{\varepsilon_i}\right) \\ a_{i,t} &= a_{i,t-1} + \eta_{i,t}, \text{ for } i = 0, \ldots, q \text{ and } \eta_{i,t} \sim \left(0, \sigma^2_{\eta_i}\right). \end{aligned} \tag{5}$$

As before, we test for the random walk property using the LaMotte–McWorther test. In addition, for structural breaks, we employ the fluctuation test [32]. Finally, we use our previous general-to-specific approach to estimate (4), starting off with lag lengths of 9 and $p = q$, and dropping those lags that were never significant (as we did before).

Having estimated the coefficients in (4), we can calculate the gain, coherence, and cross spectra based on the time-varying spectra just obtained. A direct estimation of the cross spectra is a particular problem in the case of structural breaks since the subsamples would typically be too small to allow the associated spectra to be directly estimated.

For the cross-spectral analysis, we use the methods introduced in Hughes Hallett and Richter [36]–[38]. The time-varying cross spectrum $f_{YX}(\omega)_t$ using the FFT can be written as

$$f_{YX}(\omega)_t = |T(\omega)|_t \, f_{XX}(\omega)_t \tag{6}$$

where $T(\omega)_t$ is the transfer or filter function defined in (6) and calculated as follows:

$$T(\omega)_t = \left(\frac{\sum_{b=0}^{q} a_{b,t} \exp(-j\omega b)}{1 - \sum_{i=1}^{p} v_{i,t} \exp(-j\omega i)} \right), \text{ for } t = 1, \ldots, T. \tag{7}$$

In (7), a's and v's are estimated using (4). The last term in (6), i.e., $f_{XX}(\omega)_t$, is the spectrum of the predetermined variable. This spectrum may be time varying as well (see above). However, in this paper, we are interested in the coherence and in the composition of the changes to that coherence over time. Thus, we need to establish expressions for the coherence and gain between x_t and y_t to show the degree of association and size

of impact of x_t on y_t. The spectrum of any dependent variable is defined as (e.g., [39])

$$f_{YY}(\omega)_t = |T(\omega)_t|^2 \; f_{XX}(\omega)_t + f_{vv}(\omega)_t. \tag{8}$$

From (3), we get the time-varying residual spectrum

$$f_{vv}(\omega)_t = \frac{f_{uu}(\omega)_t}{\left|1 - \sum_{i=1}^{p} v_{i,t} \exp(-j\omega i)\right|^2} \tag{9}$$

and the gain as $A(\omega)_t = |T(\omega)_t|^2$ and is calculated as described in (7).

Finally, given knowledge of $f_{YY}(\omega)_t$, $|T(\omega)_t|^2$, and $f_{XX}(\omega)_t$, we can *calculate* the coherence at each frequency as follows (as defined in Hughes Hallett and Richter [37], [40]:

$$K^2_{YX,t} = \frac{1}{\left\{1 + f_{VV}(\omega)_t / \left(|T(\omega)_t|^2 f_{XX}(\omega)_t\right)\right\}}. \tag{10}$$

The spectral coherence K^2_{XY} is a statistic that can be used to examine the relation between two signals or data sets. Values of the coherence will always satisfy $0 \leq K^2_{XY} \leq 1$. For a strictly proportional linear system with a single input x_t and single output y_t, the coherence will be equal to one. If x_t and y_t are completely unrelated, then the coherence will be zero. If K^2_{XY} is less than one but greater than zero, it is an indication that output y_t is being produced by input x_t, as well as by other inputs. Hence, the coherence is nothing else than the R^2 in the frequency domain. Since we are calculating the coherence using the short-time Fourier transform, the coherence may be also time varying. Thus, we have to extend K^2_{XY} by a time index. For the rest of this paper, we will write $K^2_{XY,t}$.

For example, if the coherence has a value of 0.6 at a frequency of 1.2, then it means that the temperature cycle at a frequency of 1.2 determines an NDVI-based vegetation growth cycle at that point in time by 60%. Similarly, a gain of 0.5 means that half the variance in temperature cycle at that frequency is transmitted to the NDVI.

IV. Results

A. NDVI-Based Growth of Semi-Natural Grassland and Climate

As mentioned before, instead of analyzing the level of NDVI, we analyze its growth rate. Fig. 2 shows the annual growth rate of NDVI. The aggregation of the ten-day data for the period 1999–2010 results in 48 seasons (12 years × 4 seasons/year).

Interestingly, the growth rate fluctuates between +15% and −15% (see Fig. 2). Seasonal effects are visible but maybe not as clear-cut as one would have expected. Although it does hold that in winter the growth rate is usually negative, it is not always positive in spring. Fig. 3 presents the growth rate of NDVI for spring time only.

For the first half of the sample, there seems to be a two-year cycle: starting in 1999, the growth rate is positive, it then becomes negative, and in 2001, it is positive again. However, one should bear in mind that a negative growth rate does not imply that vegetation is not growing in spring. It merely states that in 2000 vegetation, growth was 4% less than in 1999. In other words, a "good" year is followed by a "bad" year, which is then followed by a "good" year again.

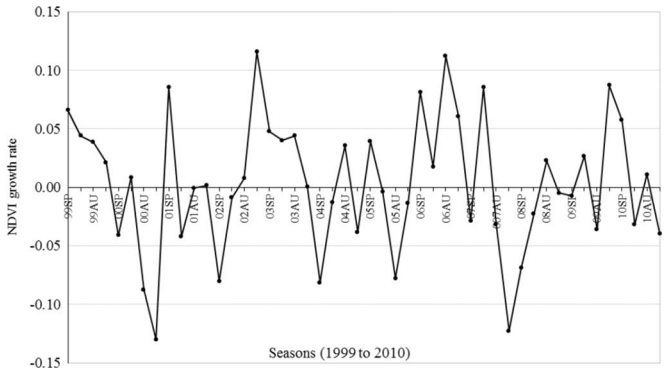

Fig. 2. Annual growth rate of NDVI for the period 1999–2000.

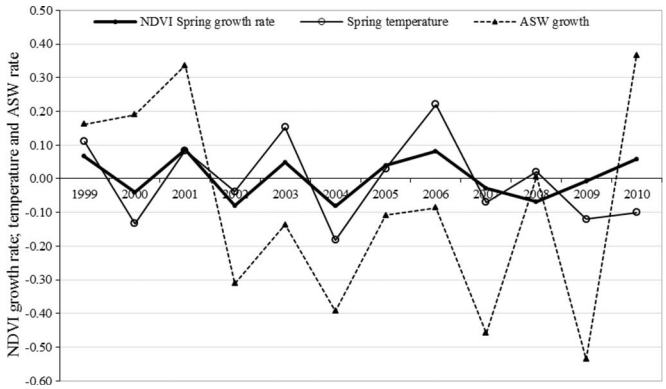

Fig. 3. Relationship between spring NDVI, temperature, and ASW growth rates for the period 1999–2010.

Importantly, from 2005 onward, the two-year cycle becomes a four-year cycle. Hence, a "good" year is followed by another good year, and this one is then followed by two "bad" years. It is worth noting that, at this stage, we cannot be sure whether this change of cycles implies a change of the temporal pattern or an irregular interannual variation. It is merely an observation without applying any statistical methods.

Remarkably, aggregation of the data reveals a symmetric behavior of the natural NDVI spring cycles as opposed to seasonal cycles. This refers to the amplitude (±8%) and the clear cyclic behavior, which also recently changed.

In the next step, we compare the spring NDVI cycles with the spring temperature cycles. A first indication of this link can be seen if we combine both growth rates of NDVI and temperature in one figure (see Fig. 3).

As in the case of the NDVI growth rate, there are two-year cycles visible up to 2007, where the cycle potentially becomes a four-year cycle. In difference to the NDVI growth rate, temperature variability is bigger. The temperature varies at some points in time (1999, 2005) by more than 15%.

The NDVI growth rate and the temperature growth rate behave in a cyclical way to each other until 2008. From 2008 onward, the link is different. In particular, for the years following 2008, it looks as if temperature and NDVI behave anticyclically with each other (see Fig. 3). Despite the obvious link of the two variables, it is remarkable that the higher fluctuation of temperature has only a reduced effect on the variability of the NDVI growth, if at all.

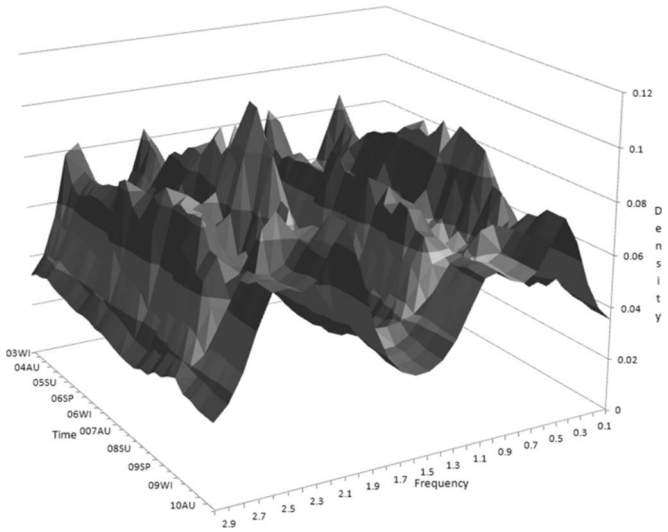

Fig. 4. Spectrum of the NDVI growth rate.

Last but not least, we also look at the growth rates of the spring NDVI and the ASW (see Fig. 3). The variability is higher than for the other two variables. The maximum is -50% in 2009. From 2001 to 2010, there is a two-year cycle visible, only once interrupted in 2005. Moreover, there also seems to be a nine-year cycle visible, namely, from 2001 to 2010.

Despite their different variability, both variables seem to move in line until 2008. As with the temperature, the relationship between NDVI and ASW should be positive.

In summary, these indicative results clearly show the existence of *natural* growth cycles. We discovered not only two-year cycles but also longer term cycles. Moreover, we could also see that the cycles are not constant. For the NDVI spring series, in particular, the two-year cycles seem to have changed to four-year cycles.

The variability of the three variables under consideration differs and so does their relationships.

The indicative results imply several issues: We need to detect which cycles are the most important one when we consider all seasons. We need a method that takes into account that cycles are not (necessarily) constant. Finally, we need a method that allows us to test the changing relationship between NDVI, soil water, and temperature.

For this reason, we decided to use a time–frequency approach that can tackle all the preceding issues. In what follows, we will shortly introduce time–frequency analysis before we apply it to the three variables.

B. Single Spectra of the NDVI Growth Rate

Fig. 4 shows the time-varying spectrum of the NDVI. The regression is based on all seasons rather than just the spring seasons, as shown earlier in this paper. For this reason, we should not necessarily expect the same cyclical behavior as in Fig. 3.

If the NDVI growth rate was a white noise process, then the spectrum would be completely flat. As one can see in Fig. 4, this is not the case. The spectrum shows peaks at the following frequencies: 0.5, 1, 2.1, and 2.5. Of these, the most important cycles are at the frequencies of 0.5 and 2.1. This corresponds to 12 and 3 seasons, respectively. The frequency of 1 corresponds to 6 seasons, and the frequency of 2.5 corresponds to 2.5 seasons.

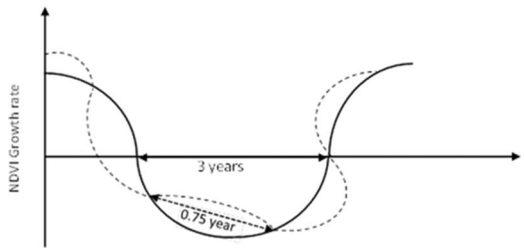

Fig. 5. Graphical interpretation of NDVI growth cycles. There are two fluctuations of equal strengths: one has a length of 3 years (solid line), and there is a shorter one of 0.75 year (dashed line).

In other words, the vegetation growth rate mainly follows 12- and 3-season cycles. Fig. 5 highlights the result.

In Fig. 5, the 12-season cycle represents 3 years and is the main cycle, whereas the 3-season cycle (or 0.75 years) fluctuates around the main cycle.

Table I shows the regression results for the series dlNDVI. This AR(8) model is the basis for the spectrum shown in Fig. 5. As one can see, the regression is robust as there is no autocorrelation. For the chosen model, this was, in fact, the lowest AIC value we could achieve. R^2 is relatively high with 99%, but there is also unexplained variance. Although the first four lags are statistically not significant at the end of the sample, they were at other sample points in time, which is why we kept them in the regression (see Table I). Hence, this table only shows the final regression for the last observation for reason of restricted space.

C. Cross-Spectra and Simulation Results

In the next step, we estimated the dependence of the NDVI growth rate on temperature and ASW rates according to (4) and (5). We used a bivariable approach in order to avoid potential multicollinearity. In other words, in the first regression, we estimated the dependence of the growth rate of NDVI on the growth rate of temperature, and in the second step, we estimated the dependence of the growth rate of NDVI on the growth rate of ASW. We start off with the temperature results.

Table II shows the regression results. As in the previous section, we only show the final observation results. All other results are available on request. The resulting coherence is shown in Fig. 6.

Fig. 6 shows that there are two cycles at which the link between the growth rate of NDVI and the temperature is biggest, namely, at frequencies of 0.8 and 2.4. These frequencies are very close to the original frequencies in Fig. 5. They correspond to cycles of 7.8 seasons (or 2 years) and 2.6 seasons (or three quarters of a year). The coherence close to these two cycles is very high as well. Thus, we can conclude that the temperature explains a lot of the spectrum apart from the short term (frequency of "π"), the long-run growth (frequency of "0"), and the cycle at a frequency of 1.6 (or 4 seasons, i.e., 1 year).

In order to analyze the NDVI-based growth rate sensitivity of the model, a number of simulations about changes in temperature and ASW were computed.

The regression results also allow us to look at the impact of a 10% change of the temperature on NDVI if everything else

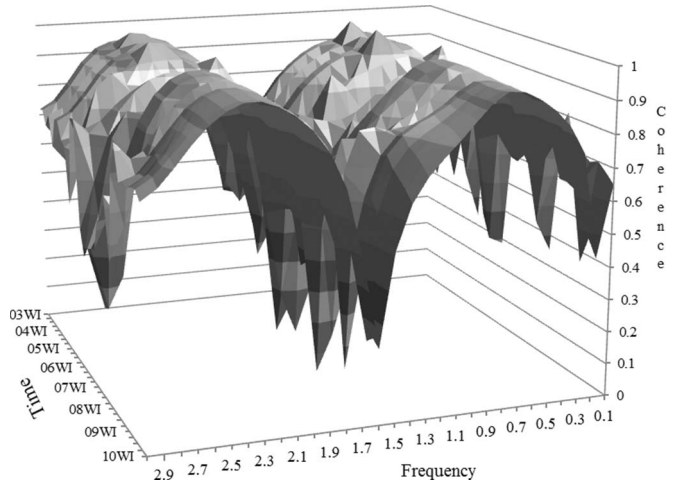

Fig. 6. Coherence between the growth rate of NDVI and the temperature.

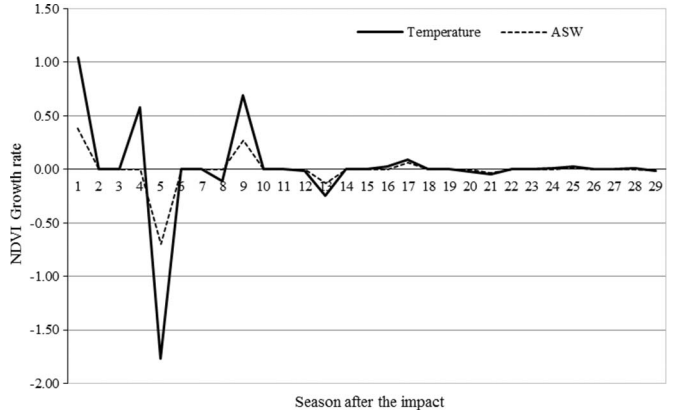

Fig. 7. Effects on the NDVI growth rate of a 10% change in the temperature and ASW growth rates.

remains constant. Fig. 7 assumes a 10% one-off increase in temperature and ASW.

Fig. 7 shows that most of the shock has been absorbed after 10 quarters, where the system returns to the steady state. From a time-series point of view, this indicates a stationary process, i.e., after a shock, the system returns to a steady-state value. It is worth noting that stationarity has not been imposed by the regression. It is the outcome of the regression, which could have been nonstationary as well.

It is interesting to note that the dynamics that are caused by a one-off increase in temperature by 10% imply positive and negative NDVI growth rates. The immediate effect of the increase in temperature is a 1% increase in the NDVI, which is followed by a 0.5% increase 4 seasons later. This increase is then completely removed in the following season, where the NDVI growth is reduced by 1.5%. These two-year cycles are in line with our observations made earlier in this paper. It is also important to note that the reaction of the NDVI growth rate to a change in temperature is underproportional to the change in temperature (about 10%).

Finally, we also analyze the impact of ASW on vegetation. We ask what NDVI growth cycles are determined by ASW. Fig. 8 gives the answer.

The coherence shown in Fig. 8 is based on the regression results in Table III. The coherence shows that the growth rate

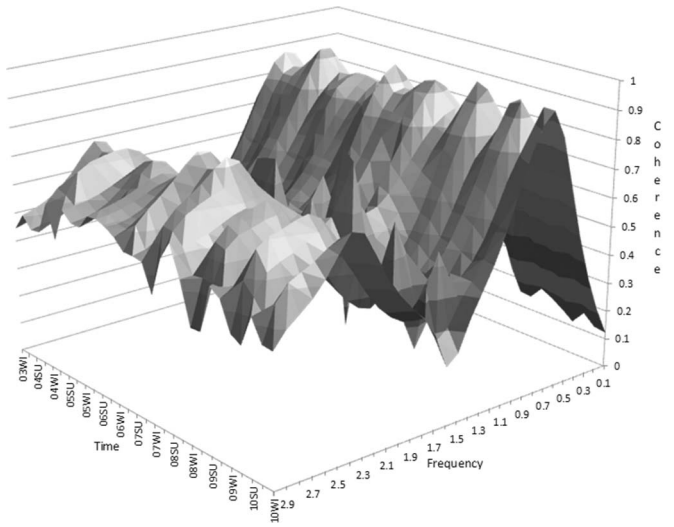

Fig. 8. Coherence between the growth rate of NDVI and the growth rate of ASW.

of the absorbed soil water explains 95% of the NDVI cycle at a frequency of 0.7, i.e., 9 seasons or 4.5 years. The second cycle the growth rate of ASW is explaining is at a frequency of 2.4 or 2.6 seasons. ASW explains about 50% of this cycle. This cycle closely corresponds to the cycle shown in Fig. 7, the spectrum of the NDVI growth rate. There is also coherence at a cycle of 1.3 of 0.5 years, but this coherence diminishes over time. The two main coherences stay important throughout the sample, although the long-run cycle coherence has slightly increased toward the end of the sample.

Overall, the mass of the spectrum, which the growth rate of ASW is explaining, is less than the temperature. Given an R^2 of 0.95, this highlights that time-series results alone may sometimes be misleading: One may not capture the crucial cycles if one only takes into account time-series properties. This is not to say that time-series results are wrong; one just has to be careful on interpreting them.

Like in the case of the temperature, we can also investigate the effects of a 10% increase in the ASW (see Fig. 7).

In Fig. 7, we can see that a 10% change in the growth rate of ASW leads to a 0.4% change in the growth rate of NDVI. Like in the case of the temperature, most adjustments have been finished after 10 seasons. Given that the behavior of the system is very similar to the temperature shock, this supports the hypothesis that a particular area can only support a certain vegetation level. From this point of view, it is certainly no coincidence that, like in the case of temperature, after 5 seasons, there is a negative effect on NDVI by about 0.6%, which is balanced four seasons later. Overall, the impact of a 10% on the NDVI growth rate is close to zero after the system returns to the steady state.

V. Discussion

The increased importance of satellite data in support of research in impact of climate on the vegetation dynamics leads to a strong need for a more comprehensive understanding of time-series changes. We apply a time–frequency approach, which not only gives us the cyclical properties but also gives how they changed over time. This alternative approach was partially

presented in previous work of Cunha and Richter [41] and Hughes Hallett and Richter [37], [40].

We achieved all of the results by estimating a dynamic time-series model. The time-series model is characterized by its lag polynomials and the time-varying weights. The lag polynomial allows us to describe the dynamic properties of the estimated relationships. As the lag polynomial is time varying itself, the Fourier transform becomes time varying. As a result, we have a time-varying spectrum and a time-varying coherence. In traditional frequency-domain analysis, a time series has to be stationary for the frequency estimators to be unbiased. By using a time-varying estimator, the series does not have to be stationary anymore as long as the nonstationarity was caused by structural breaks of which the Kalman filter is able to take care of. Therefore, with this approach, we gain more insights in the dynamic properties of a system than with the more "common" approaches (see Section I).

The results of the satellite-based grassland growth rate clearly show the existence of not only two-year spring cycles but also longer term cycles (see Figs. 2 and 3). Moreover, these cycles are not constant. In particular, the two-year cycles have changed to four-year cycles. However, if we look at the cyclical behavior of all seasons, a change of the cyclical behavior could not be observed (see Fig. 4). As a result, it seems that individual seasons may undergo cyclical changes that are offset by other seasons. This area therefore needs further research.

Our results also stated that temperature and ASW are important drivers of vegetation growth rate cycles. The variability of the three variables under consideration differs and so does their relationships. However, the link between satellite-derived vegetation growth rate and temperature is positive, as well as the link between vegetation growth rate and ASW.

We can also recognize a relative increase in importance of soil water at constant importance of temperature (see Fig. 7). Despite soil water explaining about 50% of short-term cycles, temperature still explains about 90% of those cycles. Because evapotranspiration rates are positively related to temperature, increased temperatures are likely to be associated with increased rates of soil water loss. Therefore, if temperature warms without a compensating increase in precipitation, plants may become increasingly water stressed, which could lead to decreases in growth rate where the irrigation was not possible.

The individual shocks of the temperature and ASW to the system have similar dynamic effects/consequences (see Fig. 7).

The question is what drives this behavior? Why is the growth rate of the NDVI stationary? It seems that a particular area can only support a certain vegetation level. A shock to this system can therefore only have a temporary effect, but not a permanent one, unless all other determinants of vegetation growth will support an increased vegetation, which in this scenario/regression they do not do (all other variables stayed the same). As a result, an increase in vegetation has to be offset later. The estimation results show that this offsetting starts a year later. This was not imposed in the regression and is purely a regression result. It also indicates that a shock to the system causes a two-year cycle: in the first year, vegetation increases; in the second year, it decreases.

The perennial nature of grasslands and the extensive management of soil nutrient cycles (no fertilizers added) means that soil organic matter (SOM) is a main source of soil nutrients, and thus, carry effects from year to year should be expected. Our study also shows that grass growth rates depend both on the immediate impact of the spring temperature and on the spring temperature from the previous year. As such, we hypothesize that the SOM dynamics and nitrogen cycle are intimately coupled, and temperature in mountain meadows colimits this process so that it extends for several years.

The results support the hypothesis that vegetation dynamics are physiologically dependent in several ways on the previous years. Therefore, a time-varying spectral approach, capable of separating out changes at different cyclical frequencies and points in time with respect to grassland growth, will need to provide the flexibility to capture these features and the important ecophysiological information contained therein.

VI. Conclusion

We have modeled cyclical satellite-based grassland growth rate with a time–frequency approach. It provides the cyclical properties of the satellite-based growth rate and what cycles, in particular, are explained by the climate variables.

The cyclical analysis revealed that there are more than just seasonal cycles working for the NDVI-based vegetation growth. We could show that the cyclical properties of NDVI are not constant over time.

While this time–frequency approach of satellite-based vegetation growth cycles can only give indications of causal relationships on potential climatic growth impact, they provide the catalyst for causal hypothesis generation, namely, for the plant–soil interactions, which could be tested where other data sources are available. The quantification of the relative impact of these myriad factors on the grassland dynamics is still a huge challenge for developing strategies for the sustainable use of grassland resources in northeast Portugal, as well as other extensively managed grassland systems worldwide.

Acknowledgment

The authors would like to thank the VEGETATION program for providing the satellite images. Work financed by European Regional Development Fund (ERDF), programme COMPETE and National funds by FCT-Fundação para a Ciência e a Tecnologia, project FCT EXPL/AGR-PRO/1559/2012.

References

[1] B. Boashash and A. Reilly, *Algorithms for Time–Frequency Signal Analysis*. Melbourne, Australia: Longman Cheshire, 1992, pp. 163–181.

[2] J. P. Theurillat and A. Guisan, "Potential impact of climate change on vegetation in the European Alps: A review," *Clim. Change*, vol. 50, no. 1/2, pp. 77–109, Jul. 2001.

[3] H. F. Diaz, M. Grosjean, and L. Graumlich, "Climate variability and change in high elevation regions: Past, present and future," *Clim. Change*, vol. 59, no. 1/2, pp. 1–4, Jul. 2003.

[4] M. E. Assessment, *Ecosystem and Human Wellbeing: Policy Responses*. Washington, DC, USA: Island Press, 2005.

[5] L. Telesca and R. Lasaponara, "Quantifying intra-annual persistent behaviour in SPOT_VEGETATION NDVI data for Mediterranean ecosystems of southern Italy," *Remote Sens. Environ.*, vol. 101, no. 1, pp. 95–103, Mar. 2006.

[6] P. Cayrol, A. Chehbouni, L. Kergoat, G. Dedieu, P. Mordelet, and Y. Nouvellon, "Grassland modeling and monitoring with SPOT-4 VEGETATION instrument during the 1997–1999 SALSA experiment," *Agricultural Forest Meteorol.*, vol. 105, no. 1–3, pp. 91–115, Nov. 2000.

[7] M. Cunha, A. Marcal, and L. Silva, "Very early prediction of wine yield based on satellite data from VEGETATION," *Int. J. Remote Sens.*, vol. 31, no. 12, pp. 3125–3142, Apr. 2010.
[8] I. Poças, M. Cunha, and L. Pereira, "Dynamics of semi-natural grassland meadows inferred from SPOT-Vegetation and field spectroradiometer data," *Int. J. Remote Sens.*, vol. 33, no. 14, pp. 4334–4355, Jul. 2012.
[9] M. Cunha, I. Pocas, A. R. S. Marcal, A. Rodrigues, and L. S. Pereira, "Evaluating MODIS vegetation indices using ground based measurements in mountain semi-natural meadows of northeast Portugal," *Proc. IEEE IGARSS*, pp. 1525–1528, 2010.
[10] A. Rodrigues, A. R. Marcal, and M. Cunha, "Monitoring vegetation dynamics inferred by satellite data using the PhenoSat tool," *IEEE Trans. Geosci. Remote Sens.*, vol. 51, no. 44, pp. 2096–2104, Apr. 2013.
[11] E. F. Lambin and A. H. Strahler, "Change-vector analysis in multitemporal space—A tool to detect and categorize land-cover change processes using high temporal-resolution satellite data," *Remote Sens. Environ.*, vol. 48, no. 2, pp. 231–244, May 1994.
[12] J. L. Lovell and R. D. Graetz, "Filtering pathfinder AVHRR land NDVI data for Australia," *Int. J. Remote Sens.*, vol. 22, no. 13, pp. 2649–2654, Sep. 2001.
[13] B. C. Reed, M. White, and J. F. Brown, "Remote sensing phenology," in *Phenology: An Integrative Environmental Science*. Dordrecht, The Netherlands: Kluwer, 2003, pp. 365–381.
[14] X. Y. Zhang, M. A. Friedl, C. B. Schaaf, A. H. Strahler, J. C. F. Hodges, F. Gao, B. C. Reed, and A. Huete, "Monitoring vegetation phenology using MODIS," *Remote Sens. Environ.*, vol. 84, no. 3, pp. 471–475, Mar. 2003.
[15] P. Jonsson and L. Eklundh, "TIMESAT—A program for analyzing time-series of satellite sensor data," *Comput. Geosci.*, vol. 30, no. 8, pp. 833–845, Oct. 2004.
[16] J. Chen, P. Jonsson, M. Tamura, Z. H. Gu, B. Matsushita, and L. Eklundh, "A simple method for reconstructing a high-quality NDVI time-series data set based on the Savitzky–Golay filter," *Remote Sens. Environ.*, vol. 91, no. 3/4, pp. 332–344, Jun. 2004.
[17] T. Sakamoto, M. Yokozawa, H. Toritani, M. Shibayama, N. Ishitsuka, and H. Ohno, "A crop phenology detection method using time-series MODIS data," *Remote Sens. Environ.*, vol. 96, no. 3/4, pp. 366–374, Jun. 2005.
[18] J. F. Hermance, R. W. Jacob, B. A. Bradley, and J. F. Mustard, "Extracting phenological signals from multiyear AVHRR NDVI time series: Framework for applying high-order annual splines with roughness damping," *IEEE Trans. Geosci. Remote Sens.*, vol. 45, no. 10, pp. 3264–3276, Oct. 2007.
[19] B. A. Bradley, R. W. Jacob, J. F. Hermance, and J. F. Mustard, "A curve fitting procedure to derive inter-annual phenologies from time series of noisy satellite NDVI data," *Remote Sens. Environ.*, vol. 106, no. 2, pp. 137–145, Jan. 2007.
[20] J. Verbesselt, R. Hyndman, A. Zeileis, and D. Culvenor, "Phenological change detection while accounting for abrupt and gradual trends in satellite image time series," *Remote Sens. Environ.*, vol. 114, no. 12, pp. 2970–2980, Dec. 2010.
[21] C. Atzberger and P. H. C. Eilers, "Evaluating the effectiveness of smoothing algorithms in the absence of ground reference measurements," *Int. J. Remote Sens.*, vol. 32, no. 13, pp. 3689–3709, 2011.
[22] W. Q. Zhu, Y. Z. Pan, H. He, L. L. Wang, M. J. Mou, and J. H. Liu, "A changing-weight filter method for reconstructing a high-quality NDVI time series to preserve the integrity of vegetation phenology," *IEEE Trans. Geosci. Remote Sens.*, vol. 50, no. 4, pp. 1085–1094, Apr. 2012.
[23] A. Moody and D. M. Johnson, "Land-surface phenologies from AVHRR using the discrete Fourier transform," *Remote Sens. Environ.*, vol. 75, no. 3, pp. 305–323, Mar. 2001.
[24] S. Lhermitte, J. VerBesselt, W. W. Verstraeten, and P. Coppin, "A comparison of time series similarity measures for classification and change detection of ecosystem dynamics," *Remote Sens. Environ.*, vol. 115, no. 12, pp. 3129–3152, Dec. 2011.
[25] J. N. Hird and G. J. McDermid, "Noise reduction of NDVI time series: An empirical comparison of selected techniques," *Remote Sens. Environ.*, vol. 113, no. 1, pp. 248–258, Jan. 2009.
[26] P. Coppin, I. Jonckheere, K. Nackaerts, B. Muys, and E. Lambin, "Digital change detection methods in ecosystem monitoring: A review," *Int. J. Remote Sens.*, vol. 25, no. 9, pp. 1565–1596, May 2004.
[27] J. Wang, J. J. Meng, and Y. L. Cai, "Assessing vegetation dynamics impacted by climate change in the southwestern karst region of China with AVHRR NDVI and AVHRR NPP time-series," *Environ. Geol.*, vol. 54, no. 6, pp. 1185–1195, May 2008.
[28] C. Thornthwaite and J. Mather, *The Water Balance*. Centerton, NJ, USA: Drexel Inst. Technol., Lab. Climatol., 1955.
[29] *Free VEGETATION Products*, VITO, Mol, Belgium, Nov. 5, 2011.
[30] W. H. Greene, *Econometric Analysis*. Upper Saddle River, NJ, USA: Prentice-Hall, 1997.
[31] M. Stone, "Comments on model selection criteria of Akaike and Schwarz," *J. R. Stat. Soc., Ser. B (Methodological)*, vol. 41, no. 2, pp. 276–278, 1979.
[32] W. Ploberger, W. Krämer, and K. Kontrus, "A new test for structural stability in the linear regression model," *J. Econom.*, vol. 40, no. 2, pp. 307–318, Feb. 1989.
[33] L. R. LaMotte and A. J. McWorther, "An exact test for the presence of random walk coefficients in a linear regression," *J. Amer. Stat. Assoc.*, vol. 73, no. 364, pp. 816–820, 1978.
[34] D. Gabor, "Theory of communication," *J. Inst. Elect. Eng.*, vol. 93, no. 26, pp. 429–457, Nov. 1946.
[35] Z. Lin, "An introduction to time–frequency signal analysis," *Sens. Rev.*, vol. 17, no. 1, pp. 46–53, 1997.
[36] A. Hughes Hallett and C. Richter, "Is the US no longer the economy of first resort? Changing economic relationships in the Asia–Pacific Region," *Int. Econom. Econom. Policy*, vol. 6, no. 2, pp. 207–234, Jul. 2009.
[37] A. Hughes Hallett and C. Richter, "Has there been any structural convergence in the transmission of European monetary policies?" *Int. Econom. Econom. Policy*, vol. 6, no. 2, pp. 85–101, Jul. 2009.
[38] A. Hughes Hallett and C. Richter, "Economics in the backyard: How much convergence is there between China and her special regions?" *World Econom.*, vol. 32, no. 6, pp. 819–861, Jun. 2009.
[39] J. Wolters, *Stochastic Dynamic Properties of Linear Econometric Models*. Berlin, Germany: Springer-Verlag, 1980.
[40] A. Hughes Hallett and C. Richter, "Is the convergence of business cycles a global or regional issue? The UK, US and Euroland," *J. Int. Finance Econom.*, vol. 11, no. 3, pp. 177–194, Jul. 2006.
[41] M. Cunha and C. Richter, "Measuring the impact of temperature changes on the wine production in the Douro region using the short time Fourier transform," *Int. J. Biometeorol.*, vol. 56, no. 2, pp. 357–370, Mar. 2012.

Mario Cunha was born in Grimancelos (Barcelos), Portugal. He received the M.Sc. degree in agronomic engineering from Universidade de Trás-os-Montes e Alto Douro, Villa Real, Portugal, and the Ph.D. degree in agrarian sciences from Universidade do Porto, Porto, Portugal.

He is currently an Assistant Professor with the Department of Geosciences, Environment and Spatial Planning, Faculdade de Ciências, Universidade do Porto. His research interests include various topics in remote sensing applications, agronomy, agricultural engineering, and bioclimatic environment.

Dr. Cunha was the recipient of the Syngenta Crop Protection Innovation in Agriculture Award in 2007.

Christian Richter received the Ph.D. degree in economics in 2001.

He is currently a Principal Lecturer in transnational education, economics, and management with the University of Bedfordshire, Bedfordshire, U.K. His main areas of research are behavioral economics and finance, convergence of business cycles, eurozone crisis, financial economics, time frequency analysis, and climate change.

Dr. Richter is an Honorary Chair of the International Network for Economic Research. He is an editorial board member of many scientific journals. He was a recipient of a merit award from Kingston University in 2009. He won research grants from The Leverhulme Trust and the Austrian Central Bank.